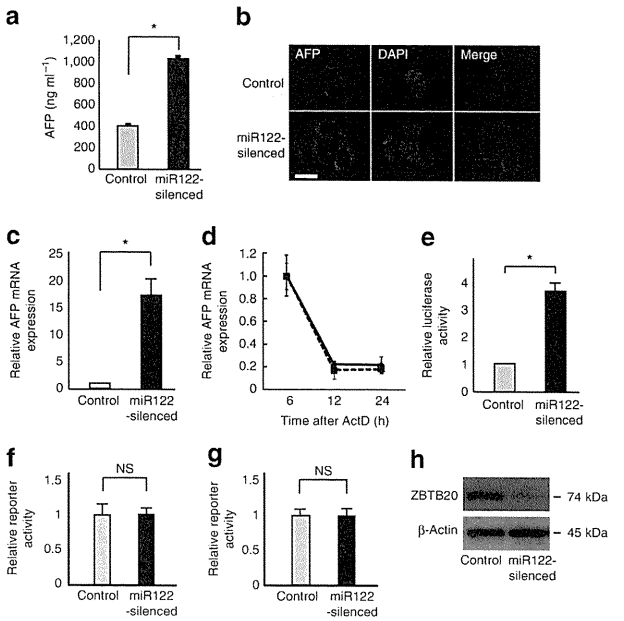

Figure 3 | Increased expression of AFP in HCC cells silenced for miR122 function. (**a**) The AFP concentration in the culture medium was determined by ELISA. Data represent the mean±s.d. of three independent experiments using Huh7 cells. $^*P<0.01$ (*t*-test). Similar results were obtained for PLC/PRF/5 cells. (**b**) Immunofluorescent staining for AFP in the cytoplasm of control and miR122-silenced Huh7cells. Representative images of stained cells from three independent experiments are shown. Scale bar, 50 μm. (**c**) Amounts of AFP mRNA in Huh7 control and miR122-silenced cells were determined by quantitative RT-PCR. Data represent the mean±s.d. of three independent experiments. $^*P<0.05$ (*t*-test). Similar results were obtained using PLC/PRF/5 cells. (**d**) AFP mRNA stability in Huh7 control (solid line) and miR122-silenced (dashed line) cells was determined by quantitative RT-PCR at 6, 12, and 24 h after treating cells with 10 μl ml^{-1} actinomycin D. Data represent the mean±s.d. of three independent experiments. Similar results were observed using PLC/PRF/5 cells. (**e**) AFP promoter activity was measured in reporter assays using Huh7 cells and AFP promoter-luciferase construct. Data represent the mean±s.d. of three independent experiments. $^*P<0.05$ (*t*-test). Similar results were obtained using PLC/PRF/5 cells. (**f**, **g**) Luciferase assays were performed using reporter plasmids to measure p53 (**f**) and β-catenin (**g**) activities. Data represent the mean±s.d. of three independent experiments. Similar results were obtained using PLC/PRF/5 cells. (**h**) ZBTB20 protein levels in miR122-silenced cells. A representative result from three independent experiments using Huh7 cells is shown. Similar results were obtained using PLC/PRF/5 cells.

in miR122-silenced cells as a result of increased AFP promoter activity. Indeed, AFP promoter activity was almost four times higher in miR122-silenced cells than in control cells, as assessed by a reporter assay (Fig. 3e).

Because AFP promoter activity is in part regulated by p53 (ref. 7), we assessed p53 activity using reporter constructs. However, no changes in p53 activity were detected in miR122-silenced cells (Fig. 3f). As mutation of β-catenin has also been reported to be involved in upregulation of AFP expression[8], we next analysed β-catenin activity in miR122-silenced cells. Similar to p53, no change in β-catenin activity was evident in miR122-silenced cells compared with control cells (Fig. 3g).

Recently, it was reported that ZBTB20 acts as a repressor of AFP transcription[9]. This result led us to assess the expression of the ZBTB20 protein in miR122-silenced cells. Indeed, western blot analysis revealed that ZBTB20 expression was decreased in miR122-silenced cells (Fig. 3h). However, as ZBT20 lacks the presence of predicted miR122 target sequences based on computational searches of the 3′-UTR, it was also unlikely that miR122 directly regulates ZBTB20 expression. These observations suggest that other indirect mechanisms may lead to decreased ZBTB20 expression in miR122-silenced cells.

CUX1 is the regulator of phenotypes in miR122-silenced cells. To explore the mechanisms by which miR122 regulates cell motility, invasion and AFP expression, we used computational searches to identify potential miR122 target genes with known functions related to these processes. This analysis led to the identification of Cut homeobox 1 (CUX1, also known as CCAAT-displacement protein/cut homeobox, CDP/Cux/Cut) through the presence of a high probability miR122 target site located in the 3′-UTR and a perfect match in the seed sequences. CUX1 is a transcription factor that regulates multiple processes including cell cycle progression, chromosomal segregation and cell migration[29,30]. Consistent with the effects of miR122 silencing described above, CUX1 was reported to modulate cell motility and invasion through the control of RhoA activity[31–33]. We observed that whereas CUX1 mRNA levels remained unchanged (Fig. 4a), there was a significant increase in the steady-state level of the CUX1 p200 and p110 isoforms in miR122-silenced cells (Fig. 4b).

To investigate the contribution of CUX1 upregulation to the increase in AFP expression and invasive properties observed in miR122-silenced cells, we knocked down CUX1 protein expression using lentiviruses expressing CUX1 short hairpin RNAs (shRNAs) (Fig. 4c). In the resulting double-knockdown cells, AFP protein expression in cell-culture supernatant and cell invasion were both reduced to levels similar to that of the parental Huh7 cells (Fig. 4d–f).

CUX1 represses ZBTB20 expression via miR214. We next assessed whether miR122 directly targets CUX1 by constructing a luciferase reporter construct that possessed a portion of the CUX1 3′-UTR containing the putative miR122 target site (Fig. 5a). Co-transfection experiments revealed that luciferase activity was suppressed by overexpression of a miR122 precursor-expressing plasmid (Fig. 5b). This suppressive effect was prevented by introducing two point mutations into the seed sequences of the miR122 target site (Fig. 5a,b), demonstrating that miR122 directly targets these sequences.

To confirm these effects, we generated 293T cell lines that stably expressed the miR122-precursor construct by transducing cells with miR122 precursor-expressing lentiviruses tagged with green fluorescent protein (Supplementary Fig. S2a). As expected, the anti-miR122 construct did not affect control 293T cells, owing to the lack of miR122 expression. However, the anti-miR122 construct greatly enhanced luciferase activity in 293T cells stably expressing the miR122-precursor, confirming that miR122 was transduced into the 293T cells (Supplementary Fig. S2b). Consistent with the results described above, these cells exhibited decreased expression of CUX1, particularly the p200 isoform, and also showed a modest, but reproducible, increase in ZBTB20 expression (Fig. 5c). These results suggest that miR122 directly regulates CUX1 protein expression, which in turn may regulate ZBTB20 expression.

Because CUX1 can function as a transcriptional modulator[29], we initially hypothesized that CUX1 is a direct regulator of ZBTB20 transcription. However, quantitative RT–PCR analysis revealed that levels of the ZBTB20 mRNA were unchanged in miR122-silenced cells compared with controls (Fig. 5d). To explain the discrepancy between unchanged levels of ZBTB20 mRNA and decreases in protein expression levels in miR122-silenced cells, we searched for miRNAs that could potentially target the ZBTB20 3′-UTR. Based on computational searches, miR214 and miR375 were identified as candidate ZBTB20-regulatory miRNAs. Although levels of miR375 were unchanged in miR122-silenced cells (Fig. 5e), expression of miR214 was significantly increased (Fig. 5e).

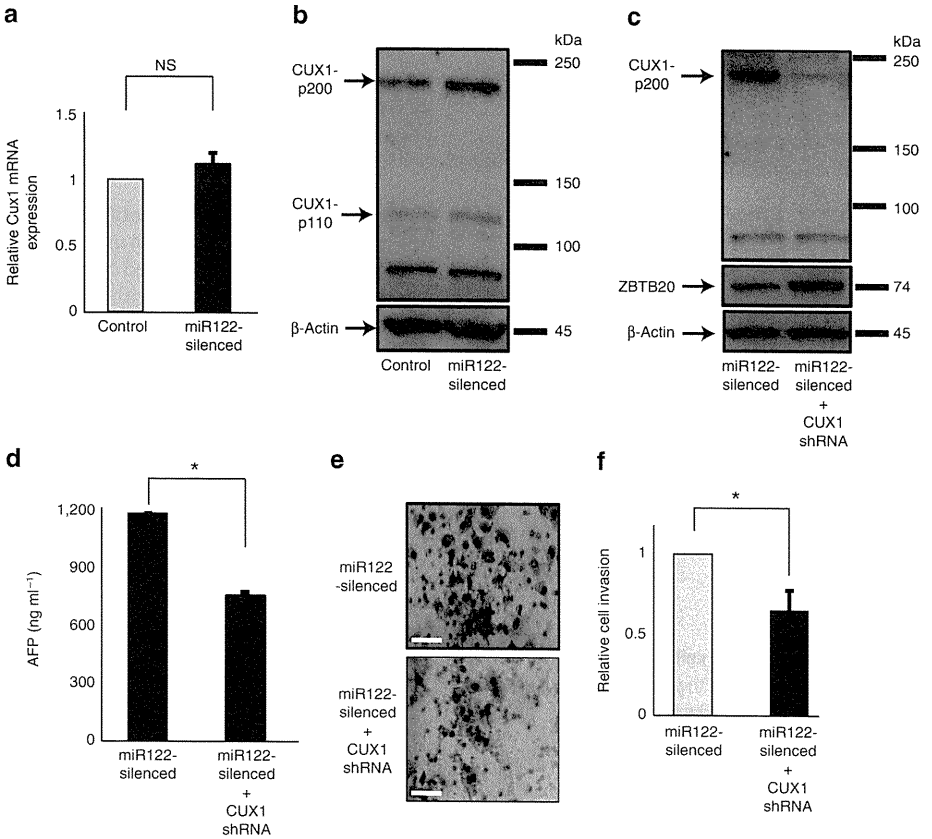

Figure 4 | CUX1-mediated regulation of AFP expression and phenotypic changes in miR122 functionally silenced cells. (**a**) CUX1 mRNA levels in control and miR122-silenced cells were analysed by quantitative RT-PCR. Data represent the mean±s.d. of three independent experiments using Huh7 cells. (**b**) p200 and p110 CUX1 protein levels were increased in miR122-silenced cells compared with control cells. A representative result from three independent experiments using Huh7 cells is shown. Similar results were obtained for PLC/PRF/5 cells. (**c**) CUX1 and ZBTB20 protein expression in double CUX1/miR122 knockdown Huh7 cells. Similar results were obtained using PLC/PRF/5 cells. (**d**) AFP concentrations in the culture medium supernatants were determined by ELISA. Data represent the mean±s.d. of three independent experiments. *$P<0.01$ (*t*-test). Similar results were observed using PLC/PRF/5 cells. (**e**, **f**) The change of cell invasion ratio by CUX1 knockdown in miR122-silenced Huh7 cells. Representative images of stained invading cells are shown (**e**). The relative cell invasion ratio after normalization to control invasion levels is shown (**f**). Data represent the mean±s.d. of three independent experiments. Scale bar, 100 μm. *$P<0.01$ (*t*-test). Similar results were obtained using PLC/PRF/5 cells.

To assess whether miR214 directly targeted the ZBTB20 3′-UTR, we constructed a luciferase reporter with the region of the ZBTB20 3′-UTR that contains the putative miR214 target site. Reporter assays revealed that luciferase activity was indeed suppressed by overexpression of the miR214 precursor, suggesting that miR214 directly targets the ZBTB20 3′-UTR and suppresses its expression (Fig. 5f). Consistent with these findings, cells that stably overexpressed the miR214 precursor exhibited decreased levels of ZBTB20 protein expression (Fig. 5g).

The putative promoter regions of miR214 contain multiple CUX1 binding sites as revealed by MATCH, a transcription factor binding site search engine (http://www.gene-regulation.com). A scanning chromatin immunoprecipitation (ChIP) experiment, followed by real-time PCR, using a series of primer pairs, confirmed that CUX1 binds to multiple genomic sites in the miR214 promoter region (Fig. 6a). We therefore hypothesized that CUX1 may regulate miR214 transcription. Consistent with this notion, we found that miR214 expression was decreased in CUX1 knockdown Huh7 cells (Fig. 6b). The role of CUX1 as an activator of miR214 transcription was further verified by knocking down or overexpressing CUX1 in another cell line. Levels of miR214 decreased following the constitutive knockdown of CUX1 with shRNA (Fig. 6c). In contrast, retroviral infection with a vector expressing p110 CUX1 led to an increase in miR214 (Fig. 6d). These findings were confirmed using doxycycline-inducible CUX1 shRNA. As previously observed for other transcriptional targets of CUX1 (refs 30,34), levels of miR214 were reduced in the presence of doxycycline, and then returned to levels higher than in untreated cells upon removal of the doxycycline inducer miR214 (Fig. 6e).

Next, to assess the contribution of miR214 to the control of ZBTB20 expression in miR122-silenced cells, we measured ZBTB20 expression after parallel silencing of miR214 in miR122-silenced cells. Although ZBTB20 protein expression was reduced by almost 50% by miR122 silencing, it was restored to >90% of control levels by miR214 silencing (Supplementary Fig. S3). Thus, CUX1-induced miR214 regulates, at least in part, ZBTB20 expression in miR122-silenced cells, leading to the upregulation of AFP expression.

Regulation of of CUX1 and AFP expression by miR122 was also confirmed in other HCC cell lines in which miR122 was overexpressed or silenced. Northern blotting showed that the expression of miR122 was relatively low in Hep3B and HepG2 cells, but was relatively high in Huh1, Huh7 and PLC/PRF/5 cells (Supplementary Fig. S4a). We therefore overexpressed the miR122 precursor in Hep3B and HepG2 cells and silenced miR122 in Huh1, Huh7 and PLC/PRF/5 cells (Supplementary Fig. S4b). CUX1 expression was respectively suppressed and enhanced by miR122 precursor overexpression and miR122 silencing (Supplementary Fig. S4c). In contrast, AFP expression was respectively enhanced and suppressed

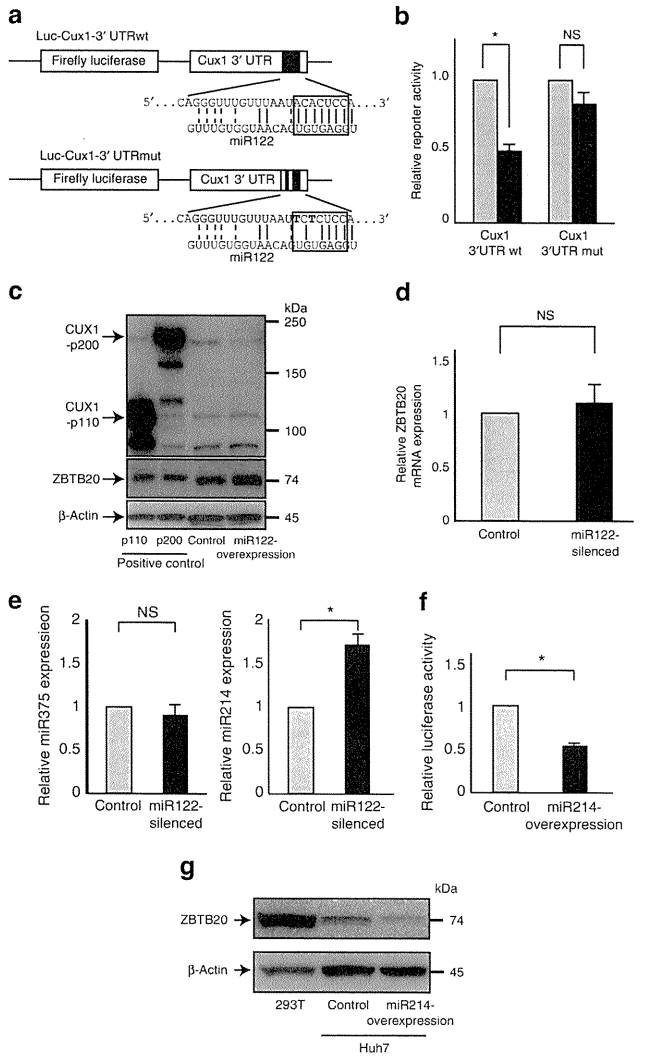

Figure 5 | MiR122 directly targets CUX1. (**a**) A luciferase reporter carrying a region of the wild type CUX1 3′UTR containing the putative miR122 target site (Luc-CUX1-3′UTRwt) was used to assess the effects of miR122 on expression of CUX1. A second luciferase reporter with two nucleotide mutations (indicated in bold) in the seed sequences (indicated by a rectangle) of the putative miR122 target sites (Luc-CUX1-3′UTRmut) was also utilized to assess specificity. (**b**) Huh7 cells were co-transfected with Luc-CUX1-3′UTRwt or Luc-CUX1-3′UTRmut and either an empty control vector (white bar) or a miR122 precursor expression plasmid (black bar). Data represent the mean±s.d. of three independent experiments. *$P<0.05$ (*t*-test). (**c**) CUX1 and ZBTB20 expression in 293T cells-expressing the miR122 precursor. Cell lysates transiently transfected with CUX1 p200 or p110 expression plasmids were used as positive controls. Representative results from four independent experiments are shown. (**d**) ZBTB20 mRNA levels in miR122-silenced Huh7 cells were determined by quantitative RT-PCR. Data represent the mean±s.d. of three independent experiments. Similar results were obtained using PLC/PRF/5 cells. (**e**) Levels of miR375 (left) and miR214 (right) in miR122-silenced Huh7 cells were analysed by quantitative RT-PCR. Data represent the mean±s.d. of three independent experiments. *$P<0.05$ (*t*-test). (**f**) Huh7 cells were co-transfected with Luc-ZBTB20-3′UTR and either an empty control vector or an miR214 precursor expression plasmid. Data represent the mean±s.d. of three independent experiments. *$P<0.05$ (*t*-test). (**g**) ZBTB20 expression was decreased in Huh7 miR214-overexpressing cells. 293T cell lysate was used as a positive control. Representative results from four independent experiments are shown.

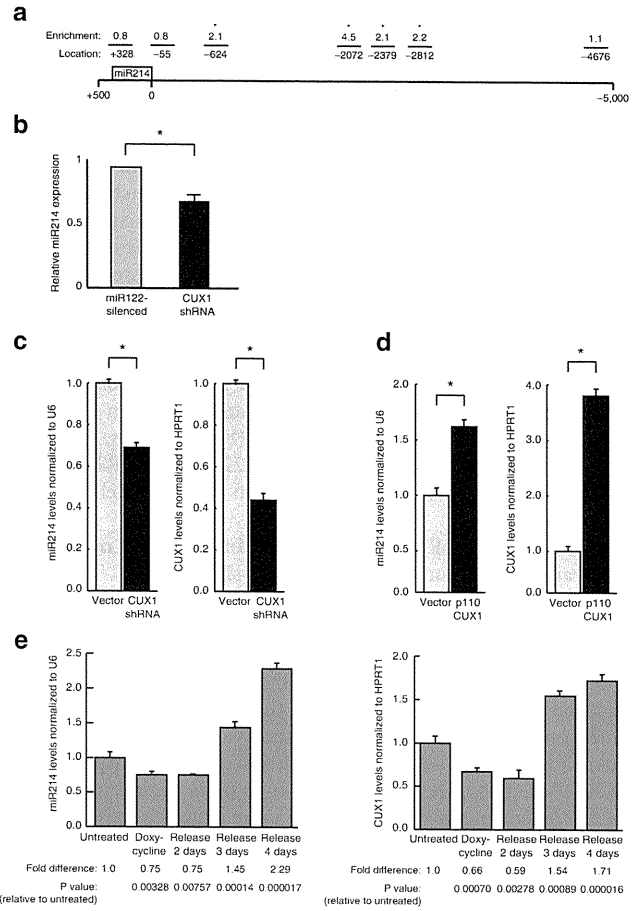

Figure 6 | CUX1 regulated miR-214 expression. (**a**), CUX1 enrichment at the miR214 locus. ChIP assays were performed using Hs578T cells. Fold enrichment and location of the center of each qPCR amplicon are shown. *$P<0.05$ (*t*-test). (**b**) MiR214 expression levels after CUX1 knockdown in miR122-silenced Huh7 cells were determined by quantitative RT-PCR. Data represent the mean±s.d. of three independent experiments. *$P<0.05$ (*t*-test). Similar results were obtained using PLC/PRF/5 cells. (**c**) Levels of miR214 and CUX1 RNA in Hs578T cells infected with an empty vector or a lentiviral vector constitutively expressing CUX1 shRNA. Data represent the mean±s.d. of three independent experiments. *$P<0.05$ (*t*-test). (**d**) Hs578T cells were infected with a retrovirus expressing p110 CUX1. Levels of miR214 and CUX1 mRNA were measured 1 day later. Data represent the mean±s.d. of three independent experiments. *$P<0.05$ (*t*-test). (**e**) Levels of miR214 and CUX1 mRNA in Hs578T cells expressing a doxycycline-inducible CUX1 shRNA. Levels are shown prior to treatment, after 5 days of doxycycline treatment, and 2, 3 and 4 days after withdrawal of doxycycline. Fold changes with the mean±s.d. of three independent experiments and *P*-values are shown (*t*-test).

(Supplementary Fig. S4d), confirming that AFP expression is regulated by an miR122-CUX1 pathway in multiple HCC cell lines.

These results indicate that functional silencing of miR122 leads to an increase in CUX1 protein expression, resulting in repression of ZBTB20 through an increase in miR214 expression. Repression of ZBTB20, in turn, leads to an increase in AFP expression. Because CUX1 is a modulator of cell motility and invasion[35–37], upregulation of this protein also enhances RhoA activity, increasing the malignant properties of cancer cells.

Expression of CUX1-related molecules in miR122-silenced mice. To explore the pathway delineated above in an *in vivo* model, we gen-

erated transgenic mice expressing antisense miR122 under the control of an H1 promoter (Fig. 7a) to inhibit the function of endogenous miR122 (ref. 38). *In situ* hybridization analysis in these mice revealed weak miR122 staining in liver tissue in comparison with control mice, likely due to binding of the anti-sense miR122 to endogenous miR122, which produces a double-stranded DNA and likely inhibits hybridization of the probe (Fig. 7b). Although structural development of the liver appeared normal based on haematoxylin and eosin staining (Supplementary Fig. S5), AFP mRNA expression (Fig. 7c) and p200 and p110 CUX1 protein expression were upregulated in the liver of anti-miR122 transgenic mice (Fig. 7d). Moreover, whereas levels of ZBTB20 mRNA were unchanged, ZBTB20 protein expression was decreased in the liver (Fig. 7d), in agreement with *in vitro* results demonstrating the regulation of ZBTB20 at the translational level (Fig. 5c,d). This was associated with a significant increase in the levels of miR214 in anti-miR122 transgenic mice (Fig. 7e). Thus, results from mouse liver tissue confirm that the miR122/CUX1/miR214/ZBTB20 regulatory pathway is also functional in an *in vivo* model.

Invasiveness of miR122-silenced cells in xenograft model. Next, we transplanted control and miR122-silenced PLC/PRF/5 cells under the liver capsule of nude mice (Fig. 7f) to determine whether miR122 silencing in HCC actually produces a more malignant phenotype *in vivo*. PLC/PRF/5 cells were chosen because of their transplantability in nude mice[39]. Neither intrahepatic metastases nor vascular invasion were detected in the livers of mice transplanted with control cells at 4 weeks post-transplantation. In contrast, vascular invasion was observed in the livers of mice transplanted with miR122-silenced HCC cells (Fig. 7g). These results suggest that miR122 silencing in HCC leads to a more aggressive phenotype.

HCC staging and the expression of miR122-related molecules. To assess the relevance of these results to human disease, we examined miR122 and AFP expression in several clinical-grade human HCC samples. We analysed miR122 expression by *in situ* hybridization (Fig. 8a) and AFP expression by immunohistochemistry (Fig. 8b). Both AFP expression and malignancy grading were inversely correlated with miR122 expression levels (Fig. 8c,d). In addition, CUX1, miR214 and ZBTB20 expression was also correlated with miR122 expression, as determined using serial sections (Supplementary Fig. S6a, b and c). These results, together with our studies in tissue culture systems and a transgenic mouse model, suggest that a reduction in the expression of miR122 increases AFP expression via a miRNA122-CUX1-miRNA214-ZBTB20 pathway and that the development of more biologically aggressive forms of HCC occurs via a miRNA122-CUX1-RhoA pathway (Supplementary Fig. S7). The miRNA-mediated mechanism described in this report may explain the clinically known link between increased AFP levels and more biologically aggressive cell characteristics in HCC.

Discussion

High AFP levels have been clinically shown to be an unfavourable prognostic factor in HCC patients[40]. In this study, we demonstrate that reduced expression of miR122 in HCC cells contributes to elevated AFP expression and, subsequently, a more aggressive phenotype. These results provide a molecular framework that explains the reported link between elevated AFP levels and a poor clinical outcome in HCC patients.

Clinically, high AFP expression is correlated with more biologically aggressive properties of HCC, as patients with high AFP levels have a significantly higher frequency of portal vein invasion and intrahepatic metastases. Additionally, these patients display significantly lower rates of recurrence-free survival and a trend towards lower overall survival[41]. In the present study, we have presented several lines of evidence indicating that decreased expression of miR122 in HCC leads to the two phenomena that

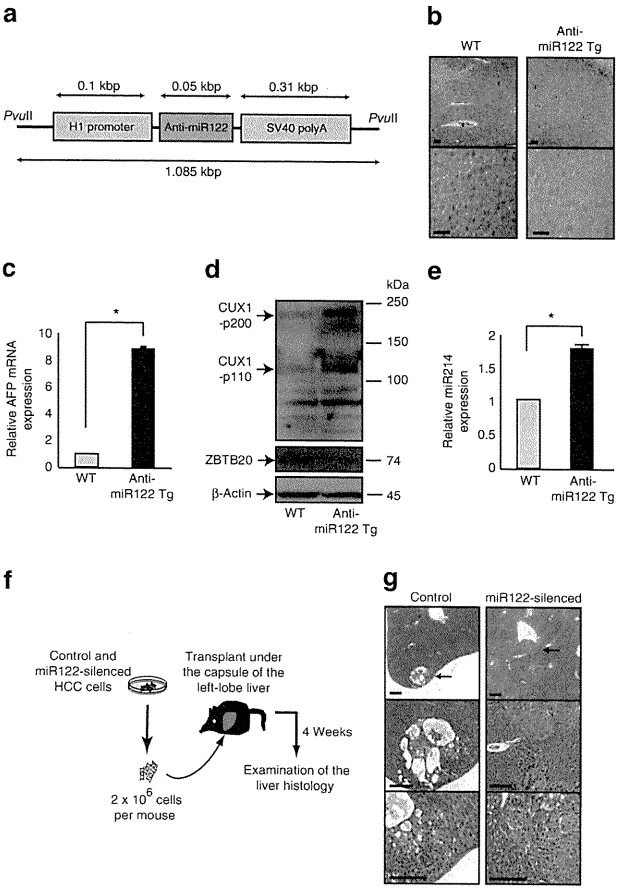

Figure 7 | AFP expression is increased in the liver of anti-miR122 transgenic mice. (**a**) DNA construct used to establishment transgenic mice in which miR122 is functionally silenced (anti-miR122 transgenic mice). This construct (like the construct used in the *in vitro* studies) generates a functional single-stranded full-length antisense miRNA complementary to miR122. (**b**) Confirmation of the expression of an antisense RNA directed against miR122 in anti-miR122 transgenic (anti-miR122 Tg) mice. Amounts of miR122 detected by *in situ* hybridization (blue/purple staining) in the liver tissues of anti-miR122 transgenic mice and WT mice. Results shown are representative of three independent experiments performed using littermates from four different mouse lines. Scale bar, 100 μm. No specific staining was observed when a negative control probe (LNA-scramble) was used. (**c**) AFP mRNA expression in mouse liver tissues was analysed by quantitative RT-PCR. Data represent the mean±s.d. of results for five mice in each group. $^*P<0.05$ (*t*-test). (**d**) CUX1 and ZBTB20 expression in mouse liver tissues was assessed by Western blotting. A representative result from three independent experiments is shown. (**e**) Levels of miR214 in liver tissues were determined by quantitative RT-PCR. Data represent the mean±s.d. of three independent experiments. $^*P<0.05$ (*t*-test). (**f**) Protocols of the orthotopic xenograft models of HCC cells. Control and miR122-silenced PLC/PRF/5 cells were prepared and injected under the capsule of the left-lobe of the nude mouse liver. Six mice were included in each group. At 4 weeks after transplantation, liver tissues were collected and sliced in series. Histological examination by H&E staining was performed to examine the tumour cell invasion status. (**g**) Representative liver histology images at 4 weeks after transplantation of tumour cells are shown. Whereas only the transplanted HCC cells beneath the capsule of the liver edge could be detected (arrow, upper left panel), neither intrahepatic metastasis nor vascular invasion was observed in the livers of mice transplanted with control cells. In contrast, vascular invasion by multiple tumour cells (arrow, upper right panel) was observed in mice transplanted with miR122-silenced cells. Scale bar, 500 μm. WT, wild type.

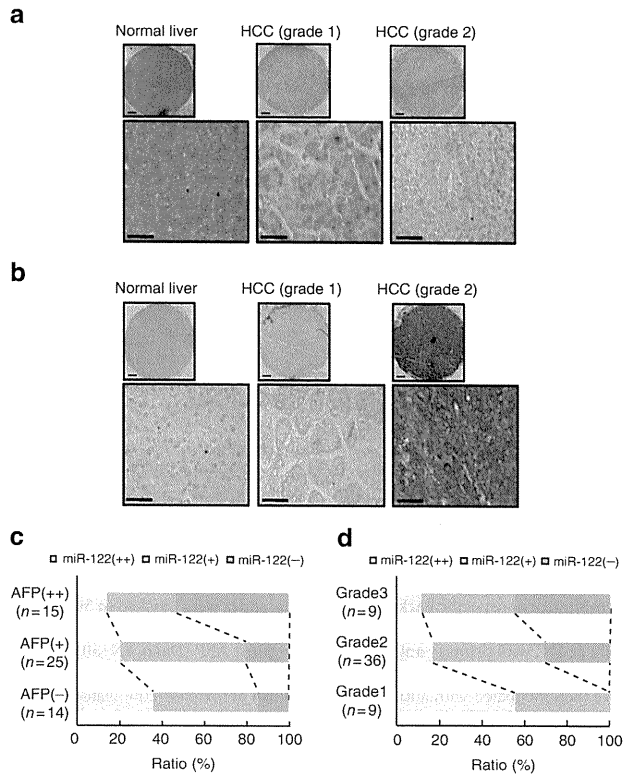

Figure 8 | AFP expression and HCC grade are inversely correlated with miR122 expression in human HCC samples. (**a**) Expression of miR122 in human clinical samples was assessed by *in situ* hybridization. Expression of miR122 (blue/purple staining) in grade 2 (more malignant) HCC samples was less than that of normal human liver tissues or grade 1 (less malignant) HCC samples. Representative images are shown. Nuclei were stained with FastRed. Scale bar, 500 μm. (**b**) AFP expression, shown in brown, was analysed by immunohistochemistry. AFP expression was higher in grade 2 HCC samples than in normal human liver tissue or grade 1 HCC samples in most cases. Representative images are shown. Scale bar, 500 μm. (**c**) Graph shows the correlation between miR122 and AFP expression. Increased AFP expression was correlated with decreased miR122 expression. (**d**) Graph shows the correlation between miR122 expression and malignancy grading of HCC. Increases in malignancy grading were correlated with decreases in miR122 expression.

are frequently observed simultaneously in the clinic: elevated expression of AFP and a more malignant biological phenotype. First, elevated AFP expression and greater cellular invasiveness were observed in miR122-knockdown cells *in vitro* and *in vivo*. Second, CUX1, which is linked with invasive characteristics in carcinoma cells[32,36,37], was shown to be involved in regulation of AFP expression and was identified as a direct target of miR122. Third, in human tissue samples from HCC patients, inverse correlations were observed between miR122 expression and AFP expression, and between miR122 expression and tumour grade. These data suggest that it is unlikely that the clinical correlation between elevated AFP levels and a more biologically aggressive phenotype in HCC is a coincidental epiphenomenon, but, instead provide a possible molecular explanation for the decrease in miR122 expression in HCC cells.

A recent study on liver development reported that liver-enriched transcription factors activate the expression of miR122, which in turn was found to promote terminal differentiation of hepatocytes through the silencing of CUX1 (ref. 42). In the present study, we confirmed that CUX1 is a direct target of miR122 and, in contrast to the situation in normal development, we showed that in grade 2 HCCs the decrease in miR122 is associated with higher CUX1 expression. High CUX1 expression was previously shown to inversely correlate with relapse-free and overall survival in high-grade breast cancers[36]. In transgenic mice, CUX1 was reported to cause various cancer-associated disorders depending on the specific isoform and tissue type expression[34,43–46]. In particular, expression of CUX1 caused organomegaly in several organs including the liver[43]. Hepatomegaly was associated with progression of lesions beginning with inflammation and leading to the development of mixed cell foci, hyperplasia and even HCCs, although in this last case statistical significance was not achieved because of the small size of the transgenic cohort[47]. The underlying mechanisms for the role of CUX1 in cancer is complex and is likely to involve both cell-autonomous and non-cell autonomous effects. However, from cell-based assays it is clear that CUX1 has a role in at least three distinct processes: cell motility, cell cycle progression and chromosome segregation[30,31,36,48]. The knockdown of CUX1 using siRNA was shown to delay entry into S phase and to hinder cell motility and invasion[31,36,48]. In contrast, overexpression of p110 CUX1 was able to accelerate S phase entry and to stimulate proliferation, migration and invasion[35,48]. Moreover, CUX1 was shown to promote genomic instability following cytokinesis failure[30]

Regulation of AFP gene expression is a complex process mediated by a number of transcriptional activators and repressors that bind the AFP gene[7,8]. ZBTB20 was recently identified as a potent repressor of AFP transcription in knockout mouse studies[9]. Our results demonstrate that decreased miR122 expression leads to concomitant decreases in ZBTB20 protein expression. This effect is mediated through upregulation of CUX1, as CUX1 silencing in miR122-silenced cells was shown to lead to both recovery of ZBTB20 levels and reduced AFP expression. Furthermore, the increased expression level of ZBTB20 in CUX1 knockdown cells suggests that ZBTB20 expression is regulated by CUX1. This miR122/CUX1/miR214/ZBTB20/AFP pathway may explain the deregulated AFP expression observed in HCC cells. Additionally, the ability of CUX1 to activate RhoA and to regulate the expression of many proteins involved in cell motility may explain the increased migration and invasiveness associated with malignancy of HCC[31–36]. It should be noted that, although this analysis revealed a trend toward inverse correlation between expression of miR122 and expression of AFP, this correlation could not be applied to all cases examined. Therefore, the possibility of additional pathways that regulate AFP expression cannot be discounted. Nonetheless, our results demonstrate that a decrease in miR122 function is a key factor that contributes to the regulation of AFP expression in HCC.

MiR122 is the most abundant miRNA in the normal adult liver, comprising approximately 80% of all miRNAs[18]. The numerous reported roles of miR122 include regulation of cholesterol biosynthesis[19,20], hepatitis C virus replication[49] and maintenance of the adult liver phenotype[21]. Specific miRNAs are often involved in the differentiation of specific cells and tissues[50]. As miR122 is liver-specific, we reasoned that this miRNA may have a role in the differentiation of normal hepatocytes. In our study, transgenic mice in which miR122 was functionally silenced were found to exhibit elevated AFP levels, but did not display abnormal morphological development in the liver (at least, not up to the age of 12 weeks), suggesting that decreased miR122 expression itself does not cause cells to become transformed. Ongoing characterization of these mice will be required to fully determine the physiological roles of miR122 in the noncancerous liver *in vivo*.

In summary, we have shown that decreased miR122 expression in HCC is linked both to more biologically aggressive tumour behaviour and elevated AFP expression. Furthermore, both of these effects were shown to be mediated by increased expression of CUX1, a direct target of miR122. Similar strategies could also be used to develop new therapeutics and diagnostics for other cancers in which miRNAs that regulate both tumour characteristics and serum markers have been identified.

Methods

Cell culture. The human HCC cell lines, Huh7, PLC/PRF/5, HepG2, Hep3B and Huh1 were obtained from the Japanese Collection of Research Bioresources. The human embryonic kidney cell line, 293T and the human breast cancer cell line HS578T were obtained from the American Type Culture Collection . All cells were maintained in Dulbecco's modified Eagle medium, supplemented with 10% fetal bovine serum.

Mouse experiments. All experiments were carried out in compliance with the regulations of the Animal Use Committee of The University of Tokyo and The Institute for Adult Disease, Asahi Life Foundation.

Generation of transgenic mice in which miR122 was functionally silenced. Mice in which miR122 function was knocked down were generated using previously described protocols[38,51]. Briefly, a DNA fragment of 1,085 bp, containing the H1 promoter region, the coding region for the antisense miR122 stem-loop-stem RNA precursor, and a transcriptional terminator of five thymidines, was resected from the miRZip-122 construct described above by digestion with *Pvu*II. Proper silencing function of the resulting DNA was confirmed via transient transfection-based reporter assays that showed efficient knockdown of miR122 function. Stable C57BL/6 embryonic stem cell lines were generated by electroporation of the linearized transgene, and the resulting cells were injected into blastocysts by the UNITECH Company. Genotyping was performed by PCR using DNA isolated from tail snips. Four different mouse lines were maintained and the male littermates were used in experiments.

Chromatin immunoprecipitation assay. ChIP for CUX1 was performed as previously described[52]. For the scanning ChIP of the miR214 locus, realtime PCR analysis was performed using primer pairs specific for different regions of the promoters. Templates for the PCR reactions were 0.1% total input DNA (I), nonspecific DNA from sepharose beads alone (S), or chipped chromatin. The respective fold enrichment of the different DNA fragments are indicated relative to the DNA obtained by purification on sepharose beads without IgG (S). Enrichment was calculated using the HPRT locus as a reference.

Doxycyclin-induced shRNA against CUX1 system. For conditional knockdown of CUX1 in Hs578t cells, we took advantage of the Addgene plasmid 11643. HS578T cells were infected with pLVCT shCUX1(5,326–5,348)-tTRKRAB lentivirus as described[53]. At 48 h after infection, cells were split and cultured with or without doxycyclin at a final concentration of 2.5 $\mu g\,ml^{-1}$. Cells were used for experiments after 5 days of treatment. Doxycyclin was then removed from the culture media and cells were maintained for 4 days following release.

Cell proliferation assay. Relative cell proliferation was assessed using a Cell Counting Kit-8 (Dojindo Laboratories), as described previously[54].

Enzyme-linked immunosorbent assay. AFP levels in the cell-culture supernatant were examined using an AFP-specific ELISA kit supplied by an outsourcing company, SRL.

Western blot analysis. Protein lysates were prepared from cells or mouse liver for immunoblot analysis. Proteins were separated by SDS–polyacrylamide gel electrophoresis and transferred to polyvinylidene difluoride membranes. After blocking with 5% dry milk to decrease nonspecific binding, membranes were probed with the appropriate primary antibodies. Primary antibodies were obtained from Abcam (ZBTB20, #ab48889, 1:500) and Santa Cruz Biotechnology (CDP, #sc-13024, 1:1,000). CUX1 antibodies (#861, 1:1,000) were generated as described previously[52]. Horseradish peroxidase-conjugated secondary antibodies were used to detect primary antibodies. Bound antibodies were detected using ECL Plus Western blotting detection reagents (GE Healthcare Life Sciences).

Scratch assay. The effects of miR122 knockdown on cellular migratory function were determined by evaluating cellular migration after scratching of a confluent monolayer of cells. Monolayers were cultured on 10 $\mu g\,ml^{-1}$ fibronectin-coated dishes and were scratched using a 200-µl pipette. Migration was analysed at the indicated time points after scratching.

***In vitro* invasion assay**. The effect of miR122 knockdown on invasive function was determined using BD BioCoat Matrigel Invasion Chambers (Becton Dickinson) according to the manufacturer's recommended protocol. Cell invasion was induced by removing the serum in the upper chamber. The number of invading cells was analysed after 22-h incubation. Cell numbers were counted in four randomly chosen fields at each time point.

Quantitative pseudopodia assay. Pseudopodium quantitation was performed using a Quantitative Pseudopodia Assay Kit (Chemicon) according to the manufacturer's instructions. Briefly, the upper chamber was coated with fibronectin and seeded with cells in serum-free medium. Serum was added to the lower chambers. 8 h later, pseudopodia on the lower surface were stained and eluted, and the absorbances of solubilized samples at 600 nm was measured using a microplate reader.

CUX1-knockdown lentiviral construct. Lentiviral particles expressing CUX1 shRNA were purchased from Santa Cruz Biotechnology (#sc-35051-V).

***In situ* hybridization to assess miR122 and miR214**. The expression of miR122 and miR214 in mouse liver and human HCC tissues was examined by *in situ* hybridization[55,56]. Locked nucleic acid (LNA)-scramble (negative control) and LNA-anti-miR122 and LNA-anti-miR214 probes were obtained from EXIQON. After deparaffinization, tissue sections were treated with 10 $\mu g\,ml^{-1}$ proteinase K for 5 min at 37 °C and refixed with 4% paraformaldehyde, followed by acetylation with 0.25% anhydrous acetic acid in 0.1 M Tris–HCl buffer (pH 8.0). Following pre-hybridization for 30 min at 48 °C, hybridization was performed overnight with each 20 nM LNA probe in hybridization buffer (5xSSC buffer, 50% formamide, 500 $\mu g\,ml^{-1}$ tRNA, 50 $\mu g\,ml^{-1}$ Cot-1 DNA). After completion of hybridization, the sections were washed with 0.1×SSC buffer for 10 min at 52 °C three times and blocked with DIG blocking buffer (Roche Diagnostics) for 30 min. Sections were then probed with anti-DIG (1:500; Roche Diagnostics) for 1 h at room temperature. Detection was performed by incubation in NBT/BCIP buffer (Promega) overnight. Nuclei were stained with Nuclear FastRed (Sigma-Aldrich).

Immunohistochemistry. Tissue arrays containing HCC tissues were purchased from US Biomax. To determine the correlations between AFP, ZBTB20, CUX1, miR122 and miR214 expression and HCC differentiation grade, slides carrying consecutive sections were obtained. Slides were baked at 65 °C for 1 h and deparaffinized. Endogenous peroxidase activity was blocked by incubation in 3% hydrogen peroxide buffer for 30 min. Antigen retrieval was performed by incubating the slides at 89 °C in 10 mM sodium citrate buffer (pH 6.0) for 30 min. To minimize nonspecific background staining, slides were blocked in 5% normal goat serum (Dako) for 10 min at room temperature. Tissues were labelled overnight at 4 °C with primary antibodies raised against AFP (Dako, #N1501, 1:100), CUX1 (#sc-13024, 1:100) and ZBTB20 (HPA016815, Sigma-Aldrich, 1:100). Slides were then incubated with anti-rabbit horseradish peroxidase-conjugated secondary antibodies (Nichirei Bioscience) for 1 h. Primary antibody binding was visualized by incubation in 3,3′-diaminobenzidine in buffered substrate (Nichirei Bioscience) for 5 min. The slides were counterstained with haematoxylin, dehydrated with ethanol, and mounted with Clarion mounting medium (Biomeda).

GTP-binding RhoA and Rac1 immunoprecipitation assay. The amount of RhoA activity was examined using an Active Rho Pull-down and Detection Kit (Thermo Fisher Scientific) according to the manufacturer's recommended protocol. The amount of GTP-bound RhoA protein (the active form of RhoA) was detected by Western blotting with the provided anti-RhoA antibody (1:100). Rac1 activity was similarly determined by using PAK-GST Protein Beads (#PAK02, Cytoskeleton) for pulldowns and anti-Rac1 antibodies (1:100) for subsequent Western blotting (#89856D, Thermo Fisher Scientific).

Orthotopic xenograft tumour model of HCC. Male BALB/c (nu/nu) nude mice were purchased from CREA Japan (Tokyo, Japan). The transplantation of tumour cells into mouse livers was performed using previously reported methods[57,58]. Briefly, 2×10^6 control or miR122-silenced PLC/PRF5 cells were suspended in 30 µl of PBS containing 1% Matrigel (Becton Dickinson). After anaesthesia, the liver was exposed through a surgical incision. Cells were slowly injected under the capsule of left lobe of the liver using a 28-gauge needle. When successful, a transparent bleb of cells could be seen through the liver capsule. After injection, light pressure was applied to the injection site with sterile gauze for 2 min to prevent bleeding and tumour cell leakage. The abdomen was then closed with sutures. Transplantation was successful in a total of 12 mice (6/group). At 4 weeks post-transplantation, liver tissues were collected, serially sectioned, and stained with haematoxylin and eosin.

Statistical analysis. Statistically significant differences between groups were determined using Student's *t*-test when variances were equal. When variances were unequal, Welch's *t*-test was used instead. *P*-values less than 0.05 were considered statistically significant.

Plasmid and stable cell line construction, reporter assays, RT–PCR, northern blotting and immunocytochemistry are described in the Supplementary Methods. All primer information is provided in Supplementary Table S1.

References

1. Parkin, D., Bray, F., Ferlay, J. & Pisani, P. Global cancer statistics, 2002. *CA Cancer J. Clin.* **55,** 74–108 (2005).
2. El-Serag, H. Epidemiology of hepatocellular carcinoma in USA. *Hepatol. Res.* **37,** S88–94 (2007).
3. Llovet, J. *et al.* Sorafenib in advanced hepatocellular carcinoma. *N. Engl. J. Med.* **359,** 378–390 (2008).
4. Greten, T. *et al.* Survival rate in patients with hepatocellular carcinoma: a retrospective analysis of 389 patients. *Br. J. Cancer* **92,** 1862–1868 (2005).
5. Greten, T., Korangy, F., Manns, M. & Malek, N. Molecular therapy for the treatment of hepatocellular carcinoma. *Br. J. Cancer* **100,** 19–23 (2009).
6. Di Bisceglie, A. Issues in screening and surveillance for hepatocellular carcinoma. *Gastroenterology* **127,** S104–S107 (2004).

7. Ogden, S. *et al. p53* targets chromatin structure alteration to repress alpha-fetoprotein gene expression. *J. Biol. Chem.* **276,** 42057–42062 (2001).
8. Peng, S. *et al.* High alpha-fetoprotein level correlates with high stage, early recurrence and poor prognosis of hepatocellular carcinoma: significance of hepatitis virus infection, age, p53 and beta-catenin mutations. *Int. J. Cancer.* **112,** 44–50 (2004).
9. Xie, Z. *et al.* Zinc finger protein ZBTB20 is a key repressor of alpha-fetoprotein gene transcription in liver. *Proc. Natl Acad. Sci. USA* **105,** 10859–10864 (2008).
10. Oishi, K. *et al.* Clinicopathologic features of poorly differentiated hepatocellular carcinoma. *J. Surg. Oncol.* **95,** 311–316 (2007).
11. Yamamoto, K. *et al.* AFP, AFP-L3, DCP, and GP73 as markers for monitoring treatment response and recurrence and as surrogate markers of clinicopathological variables of HCC. *J. Gastroenterol.* **45,** 1272–1282 (2010).
12. Matsumoto, Y. *et al.* Clinical classification of hepatoma in Japan according to serial changes in serum alpha-fetoprotein levels. *Cancer* **49,** 354–360 (1982).
13. Lee, R., Feinbaum, R. & Ambros, V. The *C. elegans* heterochronic gene lin-4 encodes small RNAs with antisense complementarity to lin-14. *Cell* **75,** 843–854 (1993).
14. Carrington, J. & Ambros, V. Role of microRNAs in plant and animal development. *Science* **301,** 336–338 (2003).
15. Bartel, D. MicroRNAs: genomics, biogenesis, mechanism, and function. *Cell* **116,** 281–297 (2004).
16. Ambros, V. The functions of animal microRNAs. *Nature* **431,** 350–355 (2004).
17. Lu, J. *et al.* MicroRNA expression profiles classify human cancers. *Nature* **435,** 834–838 (2005).
18. Landgraf, P. *et al.* A mammalian microRNA expression atlas based on small RNA library sequencing. *Cell* **129,** 1401–1414 (2007).
19. Krützfeldt, J. *et al.* Silencing of microRNAs *in vivo* with 'antagomirs'. *Nature* **438,** 685–689 (2005).
20. Esau, C. *et al.* miR-122 regulation of lipid metabolism revealed by *in vivo* antisense targeting. *Cell Metab.* **3,** 87–98 (2006).
21. Gatfield, D. *et al.* Integration of microRNA miR-122 in hepatic circadian gene expression. *Genes Dev.* **23,** 1313–1326 (2009).
22. Yan, D. *et al.* MicroRNA-1/206 targets c-Met and inhibits rhabdomyosarcoma development. *J. Biol. Chem.* **284,** 29596–29604 (2009).
23. Kutay, H. *et al.* Downregulation of miR-122 in the rodent and human hepatocellular carcinomas. *J. Cell. Biochem.* **99,** 671–678 (2006).
24. Coulouarn, C., Factor, V., Andersen, J., Durkin, M. & Thorgeirsson, S. Loss of miR-122 expression in liver cancer correlates with suppression of the hepatic phenotype and gain of metastatic properties. *Oncogene* **28,** 3526–3536 (2009).
25. Tsai, W. *et al.* MicroRNA-122 a tumor suppressor microRNA that regulates intra-hepatic metastasis of hepatocellular carcinoma. *Hepatology* **49,** 1571–1582 (2009).
26. Varnholt, H. *et al.* MicroRNA gene expression profile of hepatitis C virus-associated hepatocellular carcinoma. *Hepatology* **47,** 1223–1232 (2008).
27. Wong, Q. *et al.* MicroRNA-223 is commonly repressed in hepatocellular carcinoma and potentiates expression of Stathmin1. *Gastroenterology* **135,** 257–269 (2008).
28. Sahai, E. & Marshall, C. RHO-GTPases and cancer. *Nat. Rev. Cancer* **2,** 133–142 (2002).
29. Sansregret, L. & Nepveu, A. The multiple roles of CUX1: insights from mouse models and cell-based assays. *Gene* **412,** 84–94 (2008).
30. Sansregret, L. *et al.* Cut homeobox 1 causes chromosomal instability by promoting bipolar division after cytokinesis failure. *Proc. Natl Acad. Sci. USA* **108,** 1949–1954 (2011).
31. Kedinger, V. & Nepveu1, A. The roles of CUX1 homeodomain proteins in the establishment of a transcriptional program required for cell migration and invasion. *Cell Adh. Migr.* **4,** 348–352 (2010).
32. Michl, P., Knobel, B. & Downward, J. CUTL1 is phosphorylated by protein kinase A, modulating its effects on cell proliferation and motility. *J. Biol. Chem.* **281,** 15138–15144 (2006).
33. Seguin, L. *et al.* CUX1 and E2F1 regulate coordinated expression of the mitotic complex genes Ect2, MgcRacGAP, and MKLP1 in S phase. *Mol. Cell Biol.* **29,** 570–581 (2009).
34. Kedinger, V. *et al.* p110 CUX1 homeodomain protein stimulates cell migration and invasion in part through a regulatory cascade culminating in the repression of E-cadherin and occludin. *J. Biol. Chem.* **284,** 27701–27711 (2009).
35. Michl, P. *et al.* CUTL1 is a target of TGF(beta) signaling that enhances cancer cell motility and invasiveness. *Cancer Cell* **7,** 521–532 (2005).
36. Aleksic, T. *et al.* CUTL1 promotes tumor cell migration by decreasing proteasome-mediated Src degradation. *Oncogene* **26,** 5939–5949 (2007).
37. Kunath, T. *et al.* Transgenic RNA interference in ES cell-derived embryos recapitulates a genetic null phenotype. *Nat. Biotechnol.* **21,** 559–561 (2003).
38. Shouval, D. *et al.* Tumorigenicity in nude mice of a human hepatoma cell line containing hepatitis B virus DNA. *Cancer Res.* **41,** 1342–1350 (1981).
39. Nomura, F., Ohnishi, K. & Tanabe, Y. Clinical features and prognosis of hepatocellular carcinoma with reference to serum alpha-fetoprotein levels. Analysis of 606 patients. *Cancer* **64,** 1700–1707 (1989).
40. Johnson, P., Melia, W., Palmer, M., Portmann, B. & Williams, R. Relationship between serum alpha-foetoprotein, cirrhosis and survival in hepatocellular carcinoma. *Br. J. Cancer* **44,** 502–505 (1981).
41. Xu, H. *et al.* Liver-enriched transcription factors regulate microRNA-122 that targets CUTL1 during liver development. *Hepatology* **52,** 1431–1442 (2010).
42. Ledford, A. W. *et al.* Deregulated expression of the homeobox gene Cux-1 in transgenic mice results in downregulation of p27(kip1) expression during nephrogenesis, glomerular abnormalities, and multiorgan hyperplasia. *Dev. Biol.* **245,** 157–171 (2002).
43. Brantley, J. G., Sharma, M., Alcalay, N. I. & Heuvel, G. B. Cux-1 transgenic mice develop glomerulosclerosis and interstitial fibrosis. *Kidney Int.* **63,** 1240–1248 (2003).
44. Cadieux, C. *et al.* Mouse mammary tumor virus p75 and p110 CUX1 transgenic mice develop mammary tumors of various histologic types. *Cancer Res.* **69,** 7188–7197 (2009).
45. Cadieux, C. *et al.* Polycystic kidneys caused by sustained expression of Cux1 isoform p75. *J. Biol. Chem.* **283,** 13817–13824 (2008).
46. Cadieux, C. *et al.* Transgenic mice expressing the p75 CCAAT-displacement protein/Cut homeobox isoform develop a myeloproliferative disease-like myeloid leukemia. *Cancer Res.* **66,** 9492–9501 (2006).
47. Vanden Heuvel, G. B. *et al.* Hepatomegaly in transgenic mice expressing the homeobox gene Cux-1. *Mol. Carcinog.* **43,** 18–30 (2005).
48. Sansregret, L. *et al.* The p110 isoform of the CDP/Cux transcription factor accelerates entry into S phase. *Mol. Cell Biol.* **26,** 2441–2455 (2006).
49. Jopling, C., Yi, M., Lancaster, A., Lemon, S. & Sarnow, P. Modulation of hepatitis C virus RNA abundance by a liver-specific MicroRNA. *Science* **309,** 1577–1581 (2005).
50. Taulli, R. *et al.* The muscle-specific microRNA miR-206 blocks human rhabdomyosarcoma growth in xenotransplanted mice by promoting myogenic differentiation. *J. Clin. Invest.* **119,** 2366–2378 (2009).
51. Zhou, Y. *et al.* Chimeric mouse tumor models reveal differences in pathway activation between ERBB family- and KRAS-dependent lung adenocarcinomas. *Nat. Biotechnol.* **28,** 71–78 (2010).
52. Harada, R. *et al.* Genome-wide location analysis and expression studies reveal a role for p110 CUX1 in the activation of DNA replication genes. *Nucleic Acids Res.* **36,** 189–202 (2008).
53. Szulc, J., Wiznerowicz, M., Sauvain, M. O., Trono, D. & Aebischer, P. A versatile tool for conditional gene expression and knockdown. *Nat. Methods* **3,** 109–116 (2006).
54. Maeda, S. *et al.* Ikappa B kinasebeta/nuclear factor-kappaB activation controls the development of liver metastasis by way of interleukin-6 expression. *Hepatology* **50,** 1851–1860 (2009).
55. Elmén, J. *et al.* LNA-mediated microRNA silencing in non-human primates. *Nature* **452,** 896–899 (2008).
56. Bai, S. *et al.* MicroRNA-122 inhibits tumorigenic properties of hepatocellular carcinoma cells and sensitizes these cells to sorafenib. *J. Biol. Chem.* **284,** 32015–32027 (2009).
57. Yao, X. *et al.* A novel orthotopic tumor model to study growth factors and oncogenes in hepatocarcinogenesis. *Clin. Cancer Res.* **9,** 2719–2726 (2003).
58. Kim, M. *et al.* Generation of orthotopic and heterotopic human pancreatic cancer xenografts in immunodeficient mice. *Nat. Protoc.* **4,** 1670–1680 (2009).

Acknowledgments

This work was supported by Grants-in-Aid from the Ministry of Education, Culture, Sports, Science and Technology, Japan (#22390058, #22590718, #17016016 and #20390204) (to M. Otsuka, Y. Kondo, M. Omata and K. Koike), by Health Sciences Research Grants of The Ministry of Health, Labour and Welfare of Japan (Research on Hepatitis) (to K. Koike), by grants from the Takeda Science Foundation, Astellas Foundation for Research on Metabolic Disorders, Senri Life Science Foundation, the Foundation for Promotion of Cancer Research and the Mochida Memorial Foundation for Medical and Pharmaceutical Research (to M. Otsuka), and by the grant 019389 from the Canadian Cancer Society (to A.N.).

Author contributions

K. Kojima, M. Otsuka and A.N. planned the research and wrote the paper. K. Kojima, A.T., C.V., T.Y., Y. Kondo, Y. Kang and Z.X. performed the majority of the experiments. M.A., N.K., W.Z. and A.N. contributed materials. T.K. and H.Y. supported several experiments. M. Omata and K. Koike supervised the entire project.

Additional information

Supplementary Information accompanies this paper at http://www.nature.com/naturecommunications

Competing financial interests: The authors declare no competing financial interests.

Reprints and permission information is available online at http://npg.nature.com/reprintsandpermissions/

How to cite this article: Kojima, K. *et al.* MiRNA122 is a key regulator of α-fetoprotein expression and influences the aggressiveness of hepatocellular carcinoma. *Nat. Commun.* 2:338 doi: 10.1038/ncomms1345 (2011).

Clinical Translational Research

Oncology

Oncology 2011;80:406–415
DOI: 10.1159/000330734

Received: April 19, 2011
Accepted after revision: June 15, 2011
Published online: August 15, 2011

Identification by Differential Tissue Proteome Analysis of Talin-1 as a Novel Molecular Marker of Progression of Hepatocellular Carcinoma

Hideaki Kanamori[a, b] Takao Kawakami[d, e] Kathryn Effendi[b] Ken Yamazaki[b] Taisuke Mori[b] Hirotoshi Ebinuma[a] Yohei Masugi[b] Wenlin Du[b] Keiko Nagasaka[e] Atsushi Ogiwara[e] Yutaka Kyono[e] Minoru Tanabe[c] Hidetsugu Saito[a] Toshifumi Hibi[a] Michiie Sakamoto[b]

Departments of [a]Gastroenterology, [b]Pathology and [c]Surgery, School of Medicine, Keio University, [d]Clinical Proteome Center, Tokyo Medical University, and [e]Research and Development Division, Medical ProteoScope Company, Tokyo, Japan

Key Words

Tumor progression · Liquid chromatography-tandem mass spectrometry · Immunohistochemistry · Portal vein invasion · Disease-free survival

Abstract

Objective: Hepatocellular carcinoma (HCC) is characterized by a multistage process of tumor progression. This study addressed its molecular features to identify novel protein candidates involved in HCC progression. ***Methods:*** Using liquid chromatography-tandem mass spectrometry, proteomes of 4 early HCCs and 4 non-HCC tissues derived from 2 cases of liver transplant surgery were compared with respect to the separation profiles of their tryptic peptides. Immunohistochemistry was performed on 106 HCC nodules to confirm the results of the proteomic analysis. ***Results:*** Statistical analysis of the profiles selected the peptide peaks differentiating HCC from non-HCC. A database search of the tandem mass spectrometry data from those peptide peaks identified 61 proteins, including a cytoskeletal protein, talin-1, as upregulated in HCC. Talin-1 expression levels in HCC nodules were significantly associated with the dedifferentiation of HCC ($p = 0.001$). A follow-up survey of the examined clinical cases revealed a correlation between talin-1 upregulation and a shorter time to recurrence after resection ($p = 0.039$), which may be related to the higher rate of portal vein invasion in HCCs with talin-1 up-regulation ($p = 0.029$). ***Conclusions:*** Proteomic analysis led to identification of talin-1 as a promising HCC marker. Talin-1 upregulation is associated with HCC progression and may serve as a prognostic marker.

Introduction

Hepatocellular carcinoma (HCC), like other cancers, is characterized by a multistage process of tumor progression [1]. In the initial stage, the damaged liver tissues evolve into small nodular hypercellular lesions called dysplastic nodules (DNs). These precancerous lesions develop into early HCC, defined as small, well-differentiated HCC of vaguely nodular type, and then into progressed HCC, characterized by a distinctly nodular appearance and frequent microvascular invasion. After treatment, early HCC has a longer time to recurrence and a higher 5-year survival rate than progressed HCC [2]. The long-standing confusion in differentiating early HCC from high-

KARGER

Fax +41 61 306 12 34
E-Mail karger@karger.ch
www.karger.com

0030–2414/11/0806–0406$38.00/0

Accessible online at:
www.karger.com/ocl

Michiie Sakamoto, MD, PhD
Department of Pathology
School of Medicine, Keio University
35 Shinanomachi, Shinjuku-ku, Tokyo 160-8582 (Japan)
Tel. +81 3 5363 3764, E-Mail msakamot@sc.itc.keio.ac.jp

grade DN has been minimized since stromal invasion was recognized as a diagnostic indicator for early HCC [3], but hepatocellular changes occurring during malignant transformation are still not well characterized.

Transcriptomic and proteomic analyses are useful techniques for investigating the carcinogenesis of several malignant diseases. Comparison of the gene expression profiles among early and progressed components of nodule-in-nodule type HCCs and corresponding noncancerous liver tissues resulted in identification of heat-shock protein 70 (HSP70) [4] and cyclase-associated protein 2 [5] as molecular markers of HCC. In this study, we performed proteome analysis for direct comparison of the protein composition of early HCC and non-HCC tissues obtained from whole native livers of patients who underwent living donor liver transplantation (LDLT). During the last decade, liquid chromatography (LC) directly coupled with tandem mass spectrometry (MS/MS) has been widely used for high-resolution proteome-wide analysis from a complex protein mixture [6]. The use of an improved LC-MS/MS technology with optimal tissue sampling led us to the identification of a variety of proteins up-regulated in HCC, including talin-1.

Talin-1 is a cytoskeletal protein with a molecular mass of 270 kDa, and has been shown to play a key role in a wide variety of integrin-mediated cellular events [7]. To our knowledge, there has been no report published on the relationship between talin-1 and HCC. We have successfully applied a proteomic approach to native livers of LDLT cases and showed up-regulation of talin-1 during HCC progression.

Materials and Methods

Liver Samples

HCC and noncancerous liver tissues were obtained from HCC patients at Keio University Hospital between 2003 and 2006. This study was conducted with the approval of the Ethics Committee of Keio University School of Medicine. For proteomic analysis, we used fresh whole livers from 2 HCC patients who received LDLT. Both patients had similar clinical backgrounds (males, 49 and 54 years old at the time of surgery, infected with hepatitis C virus) and were referred to Keio University Hospital after transarterial chemoembolization for multiple HCCs and hepatic deterioration into Child-Pugh score C. Immediately after resection of the whole liver, physiological saline including 2,000 units of heparin sodium was infused into the catheterized portal trunk. After confirming visually that the fluid flowing out of the common hepatic artery and the hepatic veins did not contain residual blood, the liver was sliced into 1.5-cm-thick sections with reference to the magnetic resonance imaging. Two samples of early HCC and 2 samples of noncancerous liver tissue were macroscopically separated in 0.5–1.0-cm^3 portions from each of the livers by two experienced pathologists. The noncancerous samples were derived from the areas which were not adjacent to cancerous lesions and did not contain many fibrotic components. A total of 8 liver samples (4 HCCs and 4 noncancerous tissues) were obtained from the 2 cases and kept frozen at −80°C until use. For immunohistochemical analysis, liver samples were obtained by partial hepatectomy or liver transplant surgery, consisting of 106 HCC nodules (13 well-differentiated HCCs including 7 early, 73 moderately differentiated, and 20 poorly differentiated HCCs) and 8 DNs from the total of 91 HCC patients.

Two-Dimensional Liquid Chromatography (2DLC)-MS/MS

The resected tissues were homogenized, and the homogenates were fractionated into phosphate-buffered saline (PBS) soluble and insoluble fractions [8]. An aliquot (50 μg protein) of the soluble fraction was subjected to tryptic hydrolysis in a polyacrylamide gel matrix [8, 9]. The resulting peptide mixture was extracted from the gel matrix and dried under vacuum. Peptide separation and mass measurement were carried out using 2DLC-MS/MS [10]. Briefly, in the first-dimensional strong cation exchange (SCX) LC, the peptides retained in the SCX LC column were eluted by successive injection of ammonium formate solutions (25, 50, 100, 150, 200 and 500 mM). These effluents were mixed serially with an internal standard peptide mixture consisting of 3 synthetic peptides. The second-dimensional reverse-phase (RP) LC was performed in a total 60-min acetonitrile gradient for each of the SCX LC peptide effluents. The RP LC effluent was interfaced with an electrospray ionization source in positive ion mode on an LTQ linear ion trap mass spectrometer (Thermo Fisher Scientific Inc., Waltham, Mass., USA). Protonated peptides were analyzed sequentially for MS/MS in Data-Dependent Scanning mode, consisting of a full-range scan at an m/z range of 450–2,000 and subsequent product ion scans for each of the three most intense ions in the full scan mass spectrum.

Differential Analysis of Peptide Profiles

A peptide separation profile, consisting of the ion signals characterized by RP LC elution time, full scan m/z value and full scan signal intensity was extracted from each of the RP LC-MS/MS data files. Profile compilation was carried out using an in-house program as reported [11]. Here, the signal alignment process was aided by three common signal sets derived from the three peptides spiked into each SCX LC effluent. Following signal alignment, peak detection was performed by searching the compiled signal profile. The intensity of each detected peak is the total of the signal intensities provided from the respective peptide profiles. Student's t test and heat map representation were performed for the ion signals contained in the detected peaks using Spotfire® software (TIBCO Software Inc., Palo Alto, Calif., USA).

For peptide identification, a database search was performed using Mascot® software (Matrix Science Ltd., London, UK) [12]. MS/MS data were searched for corresponding amino acid sequences in a Swiss-Prot database (http://expasy.org/sprot). Each peptide identification item was computationally associated with a profile peak containing the original precursor ion signals. Peptide identifications were considered significant for a Mascot matching score greater than 30. Identified amino acid sequences of peptides were searched for in the Swiss-Prot database to count the identical sequences in the database.

After selection of the peptide identifications under given conditions, these were grouped into each Swiss-Prot protein sequence entry. According to the fold value of signal intensity, these peptide groups were evaluated for quantitative regulation of the corresponding protein molecules. Functional classification of these proteins was based on information described in the Gene Ontology database (http://www.geneontology.org/).

Immunohistochemistry

Immunohistochemical staining was performed on formalin-fixed, paraffin-embedded tissue sections as described previously [13]. Each section was deparaffinized, rehydrated, incubated with fresh 0.3% hydrogen peroxide in methanol for 30 min at room temperature, and then washed in PBS. The sections were autoclaved at 120°C in 10 mM sodium citrate, pH 6.0, for 10 min before incubation with normal horse serum (Vector Laboratories Inc., Burlingame, Calif., USA) for 30 min. The sections were then incubated with a mouse monoclonal antibody against talin-1 (clone TA205; Millipore Co., Billerica, Mass., USA) at a dilution of 1:200 overnight at 4°C, washed with PBS, and incubated with a secondary antibody for 60 min at room temperature. Staining was evaluated by 3 pathologists. Statistical analyses were performed using SAS® software (SAS Institute Inc., Cary, N.C., USA). Disease-free survival curves were calculated from the day of resection using the Kaplan-Meier method (JMP® software, SAS Institute), and the significance of differences in survival rates between the patient groups was calculated by the log-rank test. The results of the immunohistochemical examination were compared with the microarray data of our past study [14] which are accessible from the Genome Medicine Database of Japan (GeMDBJ; https://gemdbj.nibio.go.jp/dgdb/index.do).

Results

Differential Proteome Analysis of the Compiled Peptide Profiles

From each of the 8 liver samples, 2DLC-MS/MS generated 6 peptide profiles for each of 6 salt concentrations of SCX LC (fig. 1a). The profile compilation was performed separately for each set of 6 SCX LC fractions across the 8 tissue samples, followed by peak detection of the compiled signals. From the 6 SCX LC fractions above, we obtained 2,434, 1,912, 1,819, 1,894, 1,725, and 1,533 peaks, respectively, associated with any peptide identifications. All 11,317 peaks were subjected to selection on the basis of the following conditions: (1) A Student's t test p value less than 0.1 for difference of the signal intensities between HCC and non-HCC. (2) At least 1 peptide identification, with a Mascot matching score more than 30, associated with the relevant peak. (3) Peak intensity more than 1% of the maximum peak in a compilation. After selection, the number of candidate peaks was reduced to 283, comprising 390 peptide identifications, allowing more than two significant peptide identifications in each of the selected peaks. The heat map of the 283 peaks shows successful differentiation between HCC and non-HCC (fig. 1b).

Evaluation and Classification of Tumor Marker Candidates for HCC

Following peak selection, 390 peptide identifications associated with the selected peaks were grouped according to the protein names. Of these, 288 peptide identifications were assigned to 111 groups (proteins), whereas the remaining 102 were individual peptides supported by only single peptide identification from one sample. The latter were excluded from the following analysis because of their ambiguity both for identification and quantitation of protein. According to the fold value, i.e. the ratio of HCC to non-HCC on the average signal intensities involved in a peak, these 111 peptide groups were evaluated for the quantitative regulation status of the corresponding protein molecules. When peptides with a greater than 1-fold value accounted for more than 80% in a peptide group, the corresponding protein was considered to be upregulated in HCC. A total of 61 proteins fell into this category. Accounting for less than 20% of the total, 22 proteins were categorized as downregulated. The other 28 groups were not categorized into either set. The 61 upregulated and 22 downregulated proteins were classified further by their functional and topological aspects, based on the Gene Ontology annotations as follows (table 1): 8 cytoskeletal proteins, 7 heat shock proteins (including HSP70 as upregulated in HCC), 5 major blood proteins, 53 enzymes, and 10 other proteins.

Among several categories of proteins, we primarily chose the cytoskeletal proteins for further validation, since it is generally accepted that disorders in cellular morphogenesis underpinned by the cytoskeleton are associated with tumor progression [15], and many papers addressing cytoskeletal proteins as tumor markers have been published recently [5, 16, 17]. Table 2 focuses on the six cytoskeletal proteins which we identified as upregulated in HCC: actin α/β, filamin-A, talin-1, tubulin α chain, tubulin β chain, and WD repeat-containing protein 1. Actin was identified from 3 peptides significantly upregulated in HCC, and these peptides, SYELPDGQ-VITIGNER, QEYDESGPSIVHR and IW-HHTFYNELR, are affiliated with 10, 5 and 7 genes, respectively, of the actin isoforms according to the Swiss-Prot database. Accordingly, the peptide identifications were unable to distinguish among these isoforms. This also is the case for identification of the tu-

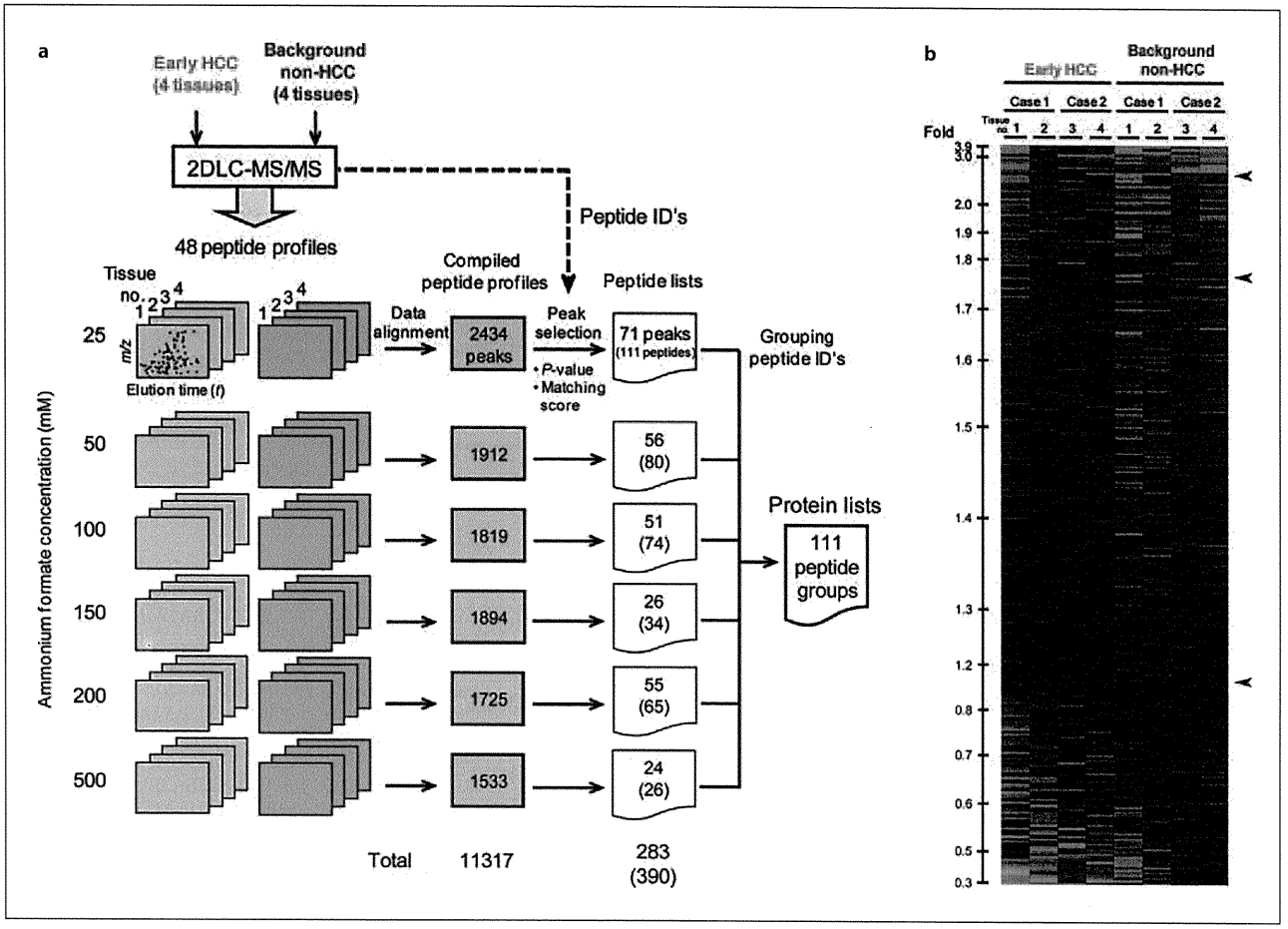

Fig. 1. Proteomic differential analysis using 2DLC-MS/MS. **a** 2DLC-MS/MS of an individual sample generated 6 peptide profiles from SCX LC peptide fractions. The profile data were compiled separately for each SCX LC fraction. This illustration shows the numbers of peaks and peptide identifications in each step. **b** Heat map representation of the 283 peptide peaks. Each color patch represents the ion signal intensity scaled to the mean of signal intensities in the corresponding peptide peak, as a continuum of relative intensity levels from green (less than 0.25-fold of the mean) to bright red (more than 2.5-fold of the mean). These peak data are shown in descending order of the fold value of early HCC to non-HCC. Arrowheads indicate the peak containing a talin-1-derived peptide.

Table 1. Classification of the candidate proteins for HCC tumor marker

Classification	Upregulated	Downregulated	Total
Cytoskeletal protein	6	2	8
Heat shock protein	6	1	7
Major blood protein	3	2	5
Enzyme	39	14	53
Others	7	3	10
Total	61	22	83

Proteins were identified from the peptides whose ion intensities varied significantly between early HCCs and non-HCC tissues ($p < 0.1$). The fold values of early HCC to non-HCC for the peptide ion intensities were used to evaluate the quantitative regulation status of the individual proteins in early HCC.

Table 2. Cytoskeletal proteins upregulated in early HCC

Protein identity (molecular weight, kDa)	Amino acid sequence of peptide	SCX LC salt concentration mM	Mascot ion score[a]	Fold value[b]	p value[c] $\times 10^2$	Swiss-Prot accession (gene name[d])	Number of Swiss-Prot accessions[e]
Actin (42)	SYELPDGQVITIGNER	25	46	1.4	8.95	A5A3E0 (A26C1B), P60709 (ACTB), P62736 (ACTA2), P63261 (ACTG1), P63267 (ACTG2), P68032 (ACTC1), P68133 (ACTA1), Q562R1 (ACTBL2), Q6S8J3 (A26C1A), Q9BYX7 (FKSG30)	10
	QEYDESGPSIVHR	100	35	1.6	2.16	A5A3E0 (A26C1B), P60709 (ACTB), P63261 (ACTG1), Q6S8J3 (A26C1A), Q9BYX7 (FKSG30)	5
	IWHHTFYNELR	200	38	1.4	9.56	A5A3E0 (A26C1B), P60709 (ACTB), P63261 (ACTG1), P68032 (ACTC1), P68133 (ACTA1), Q6S8J3 (A26C1A), Q9BYX7 (FKSG30)	7
Filamin-A (280)	IVGPSGAAVPCK	25	61	1.2	7.10	P21333 (FLNA)	1
Talin-1 (270)	LNEAAAGLNQAATELVQASR	25	35	2.4	3.71	Q9Y490 (TLN1)	1
	VQELGHGCAALVTK	50	35	1.2	4.34	Q9Y490 (TLN1)	1
	LASEAKPAAVAAENEEIGSHIK	100	54	1.7	8.37	Q9Y490 (TLN1)	1
Tubulin α chain (50)	AVFVDLEPTVIDEVR	25	81	1.9	8.43	P68363 (TUBA1B), Q71U36 (TUBA1A), Q9BQE3 (TUBA1C)	3
	AVFVDLEPTVIDEIR	100	70	2.0	2.64	P68366 (TUBA4A)	1
	LISQIVSSITASLR	100	64	1.3	6.70	P68363 (TUBA1B), P68366 (TUBA4A), Q9BQE3 (TUBA1C), Q9H853 (TUBA4B), Q9NY65 (TUBA8)	5
	IHFPLATYAPVISAEK	150	42	1.2	9.75	P68363 (TUBA1B), P68366 (TUBA4A), Q13748 (TUBA3C), Q6PEY2 (TUBA3E), Q71U36 (TUBA1A), Q9BQE3 (TUBA1C)	6
Tubulin β chain (50)	YLTVAAVFR	25	72	1.5	9.68	P04350 (TUBB4), P07437 (TUBB), P68371 (TUBB2C)	3
	SGPFGQIFRPDNFVFGQS GAGNNWAK	200	83	2.3	2.30	P04350 (TUBB4), P07437 (TUBB), P68371 (TUBB2C), Q13885 (TUBB2A), Q9BVA1 (TUBB2B)	5
WD repeat-containing protein 1 (66)	IKDIAWTEDSKR	150	45	1.3	6.76	O75083 (WDR1)	1

[a] The score (S) given as $S = -10 \times \log_{10}(P)$, where P is the absolute probability that the observed match between the MS/MS data and the amino acid sequence is a random event (http://www.matrixscience.com). [b] Signal intensity ratio of early HCC to non-HCC. [c] Significance of the difference between the ion signal intensities of early HCC and non-HCC. [d] The extract from each of the protein entries in Swiss-Prot database of Release 56.1 of September 2, 2008. [e] Protein entries containing the corresponding amino acid sequence.

bulin α and β chains, where the identified peptide sequences belong to 1 or more tubulin isoforms. Identifications of filamin-A and WD repeat-containing protein 1 were supported only by single amino acid sequences. Talin-1 was identified from 3 amino acid sequences, LNEAAAGLNQAATELVQASR, VQELGHGCAALVTK and LASEAKPAAVAAENEEIGSHIK, each being unique in the database. The relevant fold values were 2.4, 1.2 and 1.7, respectively. We focused on talin-1 because of the low ambiguity in both the identification and up-regulation. The real-time quantitative reverse transcription-polymerase chain reaction (RT-PCR) analysis of 3 LDLT cases, including the 2 cases used for the proteomic analysis, also revealed upregulation of talin-1 mRNA in HCC compared to noncancerous liver (data not shown).

Talin-1 Expression in HCC Tissue Samples

The early HCC nodules used for proteomic analyses were stained by the anti-talin-1 antibody with obvious intensity (fig. 2a). Compared with Kupffer cells, vascular smooth muscle cells, bile duct and sinusoidal endothelial

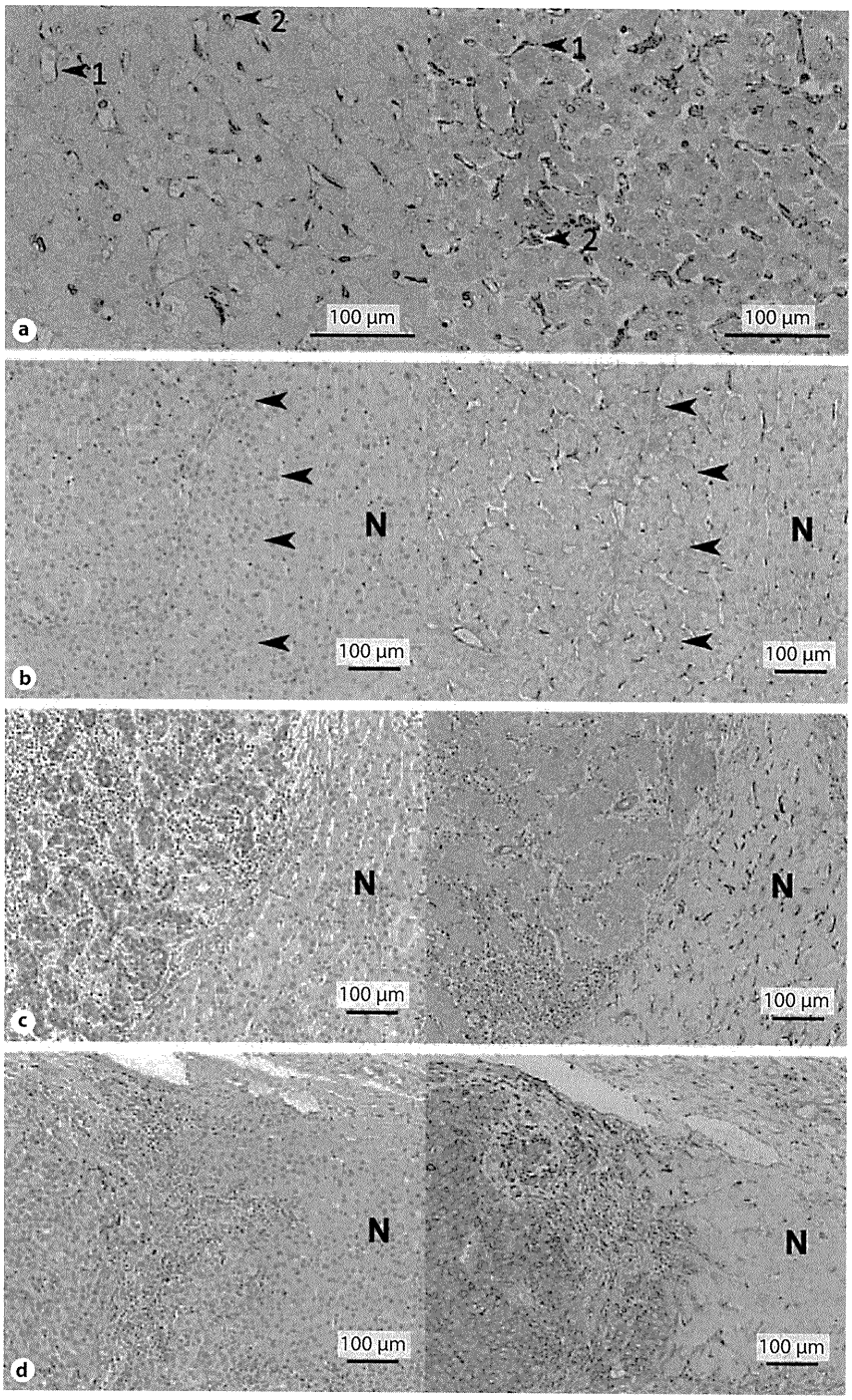

Fig. 2. Immunohistochemical analysis of talin-1. **a** Talin-1 immunostaining of tissue samples used for the proteomic analysis. Left: noncancerous liver tissue. Right: early HCC. Arrowhead 1 indicates a sinusoidal endothelial cell and arrowhead 2 a Kupffer cell. **b–d** Various histological sections were stained with hematoxylin and eosin (left plates) and anti-talin-1 antibody (right plates). **b** An early HCC with slightly stronger staining of talin-1 than the adjacent noncancerous hepatocytes. Arrowheads indicate the borders between early HCC and noncancerous liver (N). **c** A moderately differentiated HCC. **d** A poorly differentiated HCC with very strong staining of talin-1.

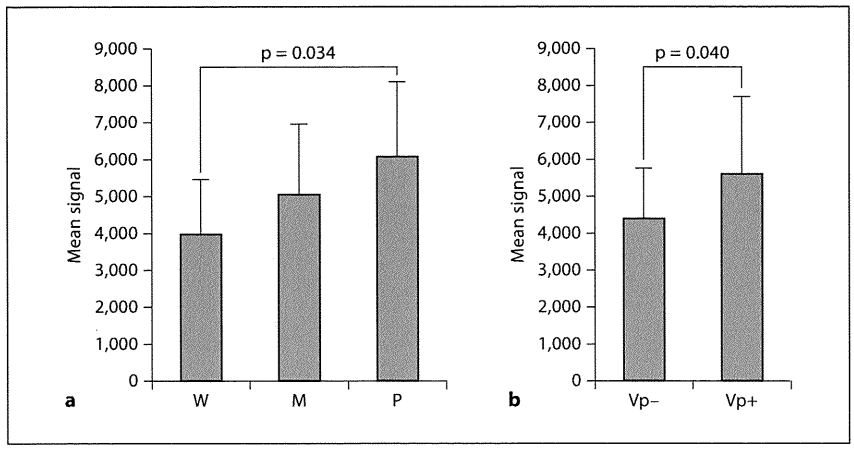

Fig. 3. Microarray analysis. **a** The means of talin-1 mRNA expression in well (W, n = 4), moderately (M, n = 23), and poorly differentiated HCCs (P, n = 13) increased in a stepwise fashion, with a significant difference between well- and poorly differentiated HCCs. **b** The average talin-1 mRNA expression was significantly up-regulated in 28 HCCs with portal vein invasion ('Vp+') as compared to 12 HCCs without portal vein invasion ('Vp–'). Error bars indicate standard deviations.

Table 3. Immunohistochemical reactivity of talin-1 with various histological patterns

Histology	Distribution of the samples according to the percentage of cells with talin-1 upregulation						p value
	<10%	10–30%	30–50%	50–70%	>70%	total	
Dysplastic nodules	4	3	0	1	0	8	
Well-differentiated HCCs (early HCCs)	3 (1)	3 (1)	2 (2)	2 (1)	3 (2)	13 (7)	0.001*
Moderately differentiated HCCs	12	12	11	14	24	73	
Poorly differentiated HCCs	2	0	1	2	15	20	

* Jonckheere-Terpstra test.

cells, which were stained by the anti-talin-1 antibody with remarkable intensity, the immunoreactivity of noncancerous hepatocytes for talin-1 was clearly weak. More intense cytoplasmic staining of the tumor cells by the anti-talin-1 antibody, compared with the adjacent hepatocytes of noncancerous liver, was considered as up-regulation of talin-1 in the tumor cells. The talin-1 immunoreactivities of 8 DNs and 106 HCC nodules are summarized in table 3. Talin-1 was significantly upregulated in early HCC cells compared with adjacent hepatocytes in noncancerous liver (Cochran-Mantel-Haenszel test, p = 0.003). The immunoreactivity of HCCs for talin-1 increased gradually according to the degree of dedifferentiation (fig. 2b–d), with statistical significance (Jonckheere-Terpstra test, p = 0.001). Poorly differentiated HCCs were characterized not only by a high percentage of cancer cells with talin-1 upregulation but also usually by a high intensity of talin-1 staining. DNs were characterized by a significantly lower percentage of talin-1 upregulation compared with all HCCs together (Cochran-Mantel-Haenszel test, p = 0.003).

We investigated the relationship between clinicopathological factors and the expression of talin-1 (table 4). The mean percentage of HCC cells with talin-1 upregulation in the examined 106 HCC nodules was 53%. We divided HCC samples into 2 groups with either more or less than 50% cancer cells showing talin-1 upregulation. As expected, the degree of cell dedifferentiation differed significantly between the 2 groups (Cochran-Mantel-Haenszel test, p = 0.004). Of great interest was the finding that HCCs containing more than 50% cancer cells with talin-1 upregulation had a significantly higher rate of portal vein invasion (Vp) than those with fewer than 50% cancer cells (Fisher's exact test, p = 0.029). In agreement with these results, the review of our past microarray data [14] showed significant upregulation of talin-1 mRNA in poorly differentiated HCCs compared with well-differentiated HCCs (Student's t test, p = 0.034), as well as in

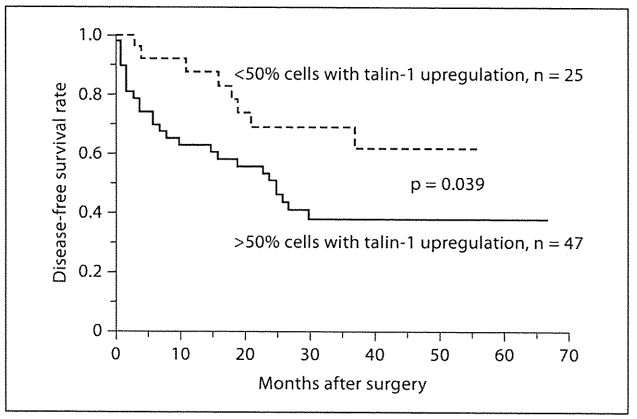

Fig. 4. Kaplan-Meier curves for disease-free survival after surgery. 47 HCC patients with greater talin-1 upregulation (solid line) had a significantly shorter disease-free survival than 25 of those with less talin-1 upregulation (dashed line).

Vp-positive HCCs compared with Vp-negative HCCs ($p = 0.040$) (fig. 3).

During a median follow-up of 25 months (range 0–67), the disease-free survival was analyzed in 72 HCC patients who underwent partial hepatectomy (fig. 4). Setting 50% cancer cells with intense immuno-staining for talin-1 as the threshold, log-rank analysis showed that 47 HCCs with greater talin-1 upregulation had a significantly shorter disease-free survival than 25 of those with less talin-1 upregulation ($p = 0.039$).

Discussion

We applied the latest proteomic technologies to early HCCs and noncancerous tissues derived from native livers of LDLT cases, resulting in identification of talin-1 as a promising candidate marker for HCC progression. In accordance with the proteomic analyses, immunohistochemical examination confirmed talin-1 upregulation in the majority of HCC cells compared with noncancerous hepatocytes. The stepwise increase of immunoreactivity for talin-1 according to the degree of dedifferentiation of HCC suggests the involvement of talin-1 in HCC progression. In general, poor prognosis of progressed HCC is associated with both high rates of intrahepatic metastasis and vascular invasion. The finding that HCCs with upregulation of talin-1 had a significantly higher rate of portal vein invasion might be associated with the shorter time to recurrence after partial hepatectomies for HCCs with talin-1 upregulation, so that the value of talin-1 as a tumor marker may be seen in prediction of clinical outcomes.

Talin-1 is one of several proteins that link the cytoplasmic domains of integrin β subunits to actin filaments [7].

Table 4. Correlations between talin-1 expression and clinical factors

Variables	Distribution of the samples (n[d]) according to the percentage of cells with talin-1 upregulation			p value[e]
	<50%	>50%	total	
Sex				0.599
Male	30	42	72	
Female	6	13	19	
Age				0.510
<60 years	12	23	35	
≥60 years	24	32	56	
Nonviral or viral (HCV + HBV)				0.083
Nonviral	13	10	23	
Viral (HCV + HBV)	23	45	68	
HCV or HBV[a]				0.422
HCV	12	30	42	
HBV	10	15	25	
Background tissue[b]				1.000
Not liver cirrhosis	20	31	51	
Liver cirrhosis	14	22	36	
Histology				0.004
Early/well-differentiated HCC	8	5	13	
Moderately differentiated HCC	35	38	73	
Poorly differentiated HCC	3	17	20	
Portal vein invasion (Vp)[c]				0.029
Vp–	26	21	47	
Vp+	19	39	58	
Intrahepatic metastasis (im)[c]				0.070
im–	38	41	79	
im+	7	19	26	

[a] One case was not counted because of infection with both HCV and HBV. [b] Four cases were not counted because of difficulty in evaluating the histology of the background tissues. [c] One sample was not counted because of difficulty in judging the presence of portal vein invasion and/or intrahepatic metastasis. [d] In the categories 'Sex', 'Age', 'Nonviral or viral', 'HCV or HBV', and 'Background tissue', n indicates the number of cases. When a case had multiple nodules, the highest percentage among the most dedifferentiated nodules was counted. In the categories 'Histology', 'Portal vein invasion', and 'Intrahepatic metastasis', n indicates the number of HCC nodules. [e] All categories were analyzed statistically with Fisher's exact test, except 'Histology' with Cochran-Mantel-Haenszel test.

Binding of talin-1 to β-integrin cytoplasmic domains is thought to trigger a conformational change in the αβ-integrin extracellular domains that increases their affinity for extracellular matrix proteins [18] and promotes assembly of focal adhesions. Talin-1 plays a pivotal role in focal adhesion dynamics, as calpain-2-mediated proteolytic cleavage of talin-1 is a rate-limiting step in focal adhesion disassembly [19]. Interactions between vinculin, talin, and actin filaments appear to constitute a slippage interface between the cytoskeleton and integrins, generating a molecular clutch that is regulated during the morphodynamic transitions of cell migration [20]. Recently, overexpression of talin-1 was reported to promote prostate cancer cell adhesion, migration and invasion [21]. Such knowledge about the cytomorphodynamic roles of talin-1 may be brought in connection with the higher incidence of portal vein invasion in HCCs with talin-1 upregulation. In addition, talin-1 also functions in signal transduction in focal adhesions, as it recruits focal adhesion kinase (FAK), which in turn recruits Src and Ras to activate downstream signaling pathways [22]. It is noteworthy that FAK itself is involved in the metastasis and invasion of HCC [23]. Recently, several molecular-targeted therapies have been developed for the treatment of various malignant diseases, and the multikinase inhibitor sorafenib has shown survival benefits in patients with advanced HCC [24]. Accumulation of knowledge about molecules such as talin-1, which may be involved in carcinogenic signaling pathways, may make available new possibilities for molecular-targeted therapy.

Besides talin-1, the 61 proteins which our proteomic analyses identified as up-regulated in HCC included HSP70, which is known as a molecular marker of HCC [4]. Filamin-A, a cytoskeletal protein listed in table 2, was recently reported to be involved in the metastasis of HCC cells [17]. Our immunohistochemical study, however, did not reveal a significant difference in filamin-A expression between HCC and noncancerous liver (data not shown). The majority of the proteins identified as up-regulated in HCC by our proteomic study still await further validation.

Proteomics has greatly contributed to the identification of specific markers for several human cancers [25]. In this work, we used a high-resolution 2DLC-MS/MS methodology for differential tissue proteome analysis. A characteristic of this strategy lies in the automated alignment of peptide signal data obtained from individual samples, which enables direct comparison of peptide signal intensities among multiple LC-MS/MS runs without any need for isotope labeling [26] and contributes to the increased reliability of analytic results. In addition, proteolytic hydrolysis of the target proteome increases the range of separable protein molecular mass, when compared to the conventional two-dimensional electrophoresis system that is based on the separation of intact proteins by their size/charge and is incapable of detecting high-molecular-mass proteins such as talin-1. It should be noted that perfusion of freshly obtained whole livers with heparinized saline resulted in depletion of body-fluid-derived, high-abundance proteins from the starting materials and, thus, enrichment of tissue proteins in the analyte. With the use of appropriately prepared materials, advanced differential tissue proteomics has the potential to detect quantitative changes of low-abundance tissue proteins which may be the key to carcinogenesis.

In conclusion, talin-1 is significantly upregulated in HCC according to tumor progression and may serve as a prognostic marker. Advanced proteomic techniques applied to freshly obtained whole native livers including early HCC portions may be a powerful method to identify unknown molecules involved in hepatocarcinogenesis.

Acknowledgements

The authors would like to thank Dr. Takeshi Kawamura, Tokyo Medical University, for his insightful supports and comments. Ms. Hisae Anyoji and Mr. Kazuya Wada, Medical Proteo-Scope Co., made enormous contributions to the analysis of the proteomics data. Special thanks also to Mr. Shinji Sato, Maze Inc., Tokyo, Japan, for his technical support of the identical sequence counting.

References

1 Takayama T, Makuuchi M, Hirohashi S, Sakamoto M, Okazaki N, Takayasu K, Kosuge T, Motoo Y, Yamazaki S, Hasegawa H: Malignant transformation of adenomatous hyperplasia to hepatocellular carcinoma. Lancet 1990;336:1150–1153.

2 Takayama T, Makuuchi M, Hirohashi S, Sakamoto M, Yamamoto J, Shimada K, Kosuge T, Okada S, Takayasu K, Yamasaki S: Early hepatocellular carcinoma as an entity with a high rate of surgical cure. Hepatology 1998;28:1241–1246.

3 International Consensus Group for Hepatocellular Neoplasia: Pathologic diagnosis of early hepatocellular carcinoma: a report of the international consensus group for hepatocellular neoplasia. Hepatology 2009;49:658–664.

4 Chuma M, Sakamoto M, Yamazaki K, Ohta T, Ohki M, Asaka M, Hirohashi S: Expression profiling in multistage hepatocarcinogenesis: identification of HSP70 as a molecular marker of early hepatocellular carcinoma. Hepatology 2003;37:198–207.
5 Shibata R, Mori T, Du W, Chuma M, Gotoh M, Shimazu M, Ueda M, Hirohashi S, Sakamoto M: Overexpression of cyclase-associated protein 2 in multistage hepatocarcinogenesis. Clin Cancer Res 2006;12:5363–5368.
6 McDonald WH, Yates JR 3rd: Shotgun proteomics: Integrating technologies to answer biological questions. Curr Opin Mol Ther 2003;5:302–309.
7 Critchley DR: Cytoskeletal proteins talin and vinculin in integrin-mediated adhesion. Biochem Soc Trans 2004;32:831–836.
8 Maeda J, Hirano T, Ogiwara A, Akimoto S, Kawakami T, Fukui Y, Oka T, Gong Y, Guo R, Inada H, Nawa K, Kojika M, Suga Y, Ohira T, Mukai K, Kato H: Proteomic analysis of stage I primary lung adenocarcinoma aimed at individualisation of postoperative therapy. Br J Cancer 2008;98:596–603.
9 Hibi T, Mori T, Fukuma M, Yamazaki K, Hashiguchi A, Yamada T, Tanabe M, Aiura K, Kawakami T, Ogiwara A, Kosuge T, Kitajima M, Kitagawa Y, Sakamoto M: Synuclein-gamma is closely involved in perineural invasion and distant metastasis in mouse models and is a novel prognostic factor in pancreatic cancer. Clin Cancer Res 2009;15:2864–2871.
10 Fujii K, Nakano T, Kanazawa M, Akimoto S, Hirano T, Kato H, Nishimura T: Clinical-scale high-throughput human plasma proteome analysis: lung adenocarcinoma. Proteomics 2005;5:1150–1159.
11 Marko-Varga G, Ogiwara A, Nishimura T, et al: Personalized medicine and proteomics: lessons from non-small cell lung cancer. J Proteome Res 2007;6:2925–2935.
12 Perkins DN, Pappin DJ, Creasy DM, Cottrell JS: Probability-based protein identification by searching sequence databases using mass spectrometry data. Electrophoresis 1999;20:3551–3567.
13 Hsu SM, Raine L, Fanger H: Use of avidin-biotin-peroxidase complex (ABC) in immunoperoxidase techniques: a comparison between ABC and unlabeled antibody (PAP) procedures. J Histochem Cytochem 1981;29:577–580.
14 Chuma M, Saeki N, Yamamoto Y, Ohta T, Asaka M, Hirohashi S, Sakamoto M: Expression profiling in hepatocellular carcinoma with intrahepatic metastasis: Identification of high-mobility group I(Y) protein as a molecular marker of hepatocellular carcinoma metastasis. Keio J Med 2004;53:90–97.
15 Hall A: The cytoskeleton and cancer. Cancer Metastasis Rev 2009;28:5–14.
16 Yamazaki K, Takamura M, Masugi Y, Mori T, Du W, Hibi T, Hiraoka N, Ohta T, Ohki M, Hirohashi S, Sakamoto M: Adenylate cyclase-associated protein 1 overexpressed in pancreatic cancers is involved in cancer cell motility. Lab Invest 2009;89:425–432.
17 Ai J, Huang H, Lv X, Tang Z, Chen M, Chen T, Duan W, Sun H, Li Q, Tan R, Liu Y, Duan J, Yang Y, Wei Y, Li Y, Zhou Q: FLNA and PGK1 are two potential markers for progression in hepatocellular carcinoma. Cell Physiol Biochem 2011;27:207–216.
18 Calderwood DA: Integrin activation. J Cell Sci 2004;117:657–666.
19 Franco SJ, Rodgers MA, Perrin BJ, Han J, Bennin DA, Critchley DR, Huttenlocher A: Calpain-mediated proteolysis of talin regulates adhesion dynamics. Nat Cell Biol 2004;6:977–983.
20 Hu K, Ji L, Applegate KT, Danuser G, Waterman-Storer CM: Differential transmission of actin motion within focal adhesions. Science 2007;315:111–115.
21 Sakamoto S, McCann RO, Dhir R, Kyprianou N: Talin1 promotes tumor invasion and metastasis via focal adhesion signaling and anoikis resistance. Cancer Res 2010;70:1885–95.
22 Chen HC, Appeddu PA, Parsons JT, Hildebrand JD, Schaller MD, Guan JL: Interaction of focal adhesion kinase with cytoskeletal protein talin. J Biol Chem 1995;270:16995–16999.
23 Chen JS, Huang XH, Wang Q, Chen XL, Fu XH, Tan HX, Zhang LJ, Li W, Bi J: FAK is involved in invasion and metastasis of hepatocellular carcinoma. Clin Exp Metastasis 2010;27:71–82.
24 Llovet JM, Bruix J: Molecular targeted therapies in hepatocellular carcinoma. Hepatology 2008;48:1312–1327.
25 Hanash SM, Pitteri SJ, Faca VM: Mining the plasma proteome for cancer biomarkers. Nature 2008;452:571–579.
26 America AH, Cordewener JH: Comparative LC-MS: a landscape of peaks and valleys. Proteomics 2008;8:731–749.

Clinical Study

Oncology

Oncology 2011;80:278–288
DOI: 10.1159/000328448

Received: November 9, 2010
Accepted after revision: February 23, 2011
Published online: July 7, 2011

Expression of Keratin 19 Is Related to High Recurrence of Hepatocellular Carcinoma after Radiofrequency Ablation

Kaoru Tsuchiya[a] Mina Komuta[b] Yutaka Yasui[a] Nobuharu Tamaki[a]
Takanori Hosokawa[a] Ken Ueda[a] Teiji Kuzuya[a] Jun Itakura[a]
Hiroyuki Nakanishi[a] Yuka Takahashi[a] Masayuki Kurosaki[a] Yasuhiro Asahina[a]
Nobuyuki Enomoto[c] Michiie Sakamoto[b] Namiki Izumi[a]

[a]Department of Gastroenterology and Hepatology, Musashino Red Cross Hospital, and [b]Department of Pathology, School of Medicine, Keio University, Tokyo, and [c]First Department of Internal Medicine, Yamanashi University School of Medicine, Yamanashi, Japan

Key Words
Hepatocellular carcinoma · Radiofrequency ablation · Recurrence · Keratin · Carcinogenesis · Needle biopsy · Hepatic progenitor cell

Abstract
Objective: Keratin (K) 19 positivity has been reported to be a useful predictive marker for recurrence in patients with hepatocellular carcinoma (HCC) who have undergone hepatic resection. We investigated the clinical usefulness of K19 positivity in patients who had received curative radiofrequency ablation (RFA). ***Methods:*** We retrospectively evaluated the clinicopathological features, including imaging and K19 expression, in 246 patients with HCC who were within the Milan criteria and had received curative RFA. Using a two-step insertion method, tumor biopsies were obtained just prior to RFA and were evaluated histologically. ***Results:*** Tumor seeding due to liver biopsy and RFA was not observed. Ten patients (4.1%) had K19-positive HCC. Imaging findings were similar between K19-positive and -negative HCC ($p = 0.187$). Nine out of 10 patients (90%) who had K19-positive HCC had recurrence of HCC after RFA, and intrahepatic recurrences were observed within 12 months in 6 out of 10 (60.0%). K19 positivity was a significant risk factor for recurrence ($p < 0.0001$) and early recurrence (<1 year after RFA; $p = 0.012$). K19 expression ($p = 0.016$) was an independent risk factor for tumor status exceeding the Milan criteria after RFA. ***Conclusion:*** Expression of K19 is related to high recurrence of HCC after curative RFA.

Introduction

Radiofrequency ablation (RFA) is regarded as an important treatment modality for hepatocellular carcinoma (HCC) [1–4], and its efficacy, especially for tumors <2 cm in diameter, is better than that of ethanol and nearly comparable to that of surgical resection [5]. In addition, RFA

Kaoru Tsuchiya and Mina Komuta contributed equally to this work.
Michiie Sakamoto and Namiki Izumi contributed equally to this work.

KARGER
Fax +41 61 306 12 34
E-Mail karger@karger.ch
www.karger.com

0030–2414/11/0804–0278$38.00/0

Accessible online at:
www.karger.com/ocl

Namiki Izumi, MD, PhD
Department of Gastroenterology and Hepatology
Musashino Red Cross Hospital
1-26-1 Kyonan-cho, Musashino-shi, Tokyo 180-8610 (Japan)
Tel. +81 422 32 3111, E-Mail nizumi@musashino.jrc.or.jp

is considered to be a bridge to liver transplantation because the prolonged waiting time for cadaveric livers leads to dropouts from the waiting list [6]. Tumor recurrence after curative RFA has been a problem, as it is after hepatic resection. Tumor size (>3 cm in diameter) [7], time after treatment (>1 year) [7], the number of HCC nodules [8] and hepatitis C virus (HCV) infection [8] have been reported to be risk factors for intrahepatic tumor recurrence after curative RFA. Moreover, primary technical failure is reported to be a risk factor for tumor progression beyond the Milan criteria after RFA [9].

Keratin (K) 19, which is considered to be a biliary/hepatic progenitor cell marker [10], has attracted attention as a useful predictive marker for detecting the more aggressive HCCs after curative resection, because tumors with K19 expression have a poorer prognosis [11, 12] and higher rates of recurrence [13, 14] and lymph node metastasis [12] than K19-negative HCC. In these previous studies, surgical specimens were investigated and K19 positivity was defined as expression in >5% of tumor cells [11–14].

As a result, one would expect that K19 expression might be a useful predictive marker for detecting HCC with a worse outcome after RFA, especially regarding tumor recurrence. To the best of our knowledge, the correlation between clinicopathological features and K19 expression has not been investigated in HCC patients treated by RFA. Therefore, we performed a clinicopathological study on 246 HCC cases treated with RFA and investigated the relationship between the K19 expression and recurrence and prognosis after treatment.

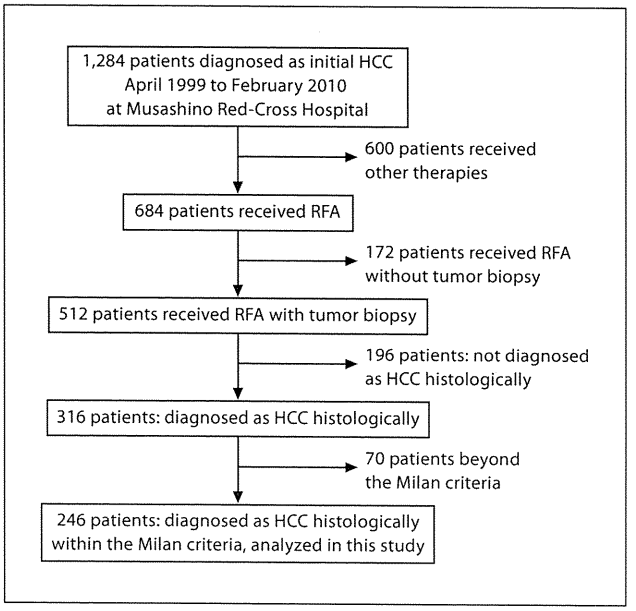

Fig. 1. Flow chart summarizing the patient selection for the study.

Methods

Patients

Between April 1999 and February 2010, 1,284 patients were admitted to the Musashino Red Cross Hospital for the first treatment of HCC. A total of 684 patients were treated with RFA as the initial therapy for HCC. Ablation therapy was chosen either because the patients were considered not to be suitable for resection (n = 323), when considering impairment of liver function, number and distribution of the tumors as well as cardiopulmonary dysfunction, or because they preferred ablation and provided informed consent (n = 361), despite surgery also being feasible. From the outset, 172 patients were excluded because RFA was performed without tumor biopsy. Therefore, 512 consecutive patients, on whom tumor biopsies had been performed before RFA, were included and we evaluated these specimens retrospectively. The result of retrospective analysis was that there were 57 patients with no residual samples, 119 patients with no tumorous lesion and 9 patients with no definitive histological diagnosis because of a small and/or fragmented specimen. The remaining specimens were diagnosed as HCC in 316 patients, as dysplastic nodule in 6 patients, as adenocarcinoma in 4 patients and as neuroendocrine tumor in 1 patient. Seventy patients were excluded, because their states of HCC were beyond the Milan criteria (≤3 cm and up to 3 nodules, or ≤5 cm and a single nodule). Therefore, 246 consecutive patients, on whom tumor biopsies had been performed before RFA and diagnosed as HCC retrospectively, were included in the study (fig. 1). The inclusion criteria for receiving RFA were as follows: total bilirubin concentration <3.0 mg/dl, platelet count >3 × 10^5/mm^3, prothrombin activity >50% (approximately equal to an international normalized ratio of 1.5) and Child-Pugh score <8 points. Ascites were controlled by administration of diuretics before RFA. Patients with macroscopic vascular invasion or extrahepatic metastases were excluded. The criteria of the International Union against Cancer were used for TNM classification [15]. Written informed consent was obtained from all patients, and the study was approved by the ethics committee at Musashino Red Cross Hospital, in accordance with the Declaration of Helsinki.

Diagnosis of HCC

All the patients were diagnosed as having HCC on the basis of tumor markers and a combination of typical imaging findings on ultrasonography (US) and dynamic computed tomography (CT), according to the American Association for the Study of Liver Diseases and the Japan Society of Hepatology guidelines [1, 16]. When patients had 2 or 3 HCC nodules, a needle biopsy was taken from the main nodule. The histological diagnosis of HCC was based on the World Health Organization criteria [17].

For the evaluation of vascularity and Kupffer cell activity of the target nodule, CT during arteriography (CTHA) and CT dur-

ing arterioportography (CTAP) were performed in 188 (76.4%) patients, superparamagnetic iron oxide-enhanced magnetic resonance imaging (SPIO-MRI) was performed in 194 (78.8%) patients and gadolinium-ethoxybenzyl-diethylenetriamine pentaacetic acid magnetic resonance imaging (Gd-EOB-DTPA) was performed in 47 patients (19.1%), from March 2008. For triple-phase dynamic CT scans, arterial, portal and equivalent phases were 35, 70 and 150 s, respectively, after injection of contrast agent. Spiral CT scans were obtained from 3- to 5-mm-thick sections. Board-certified radiologists diagnosed HCC on the basis of typical patterns, such as an early-phase hyperattenuation area and late-phase hypoattenuation on dynamic CT. According to previous studies, the sensitivity of the diagnosis of HCC in CTHA/CTAP is higher than that of spiral CT. The diagnosis of HCC in CTHA/CTAP is hyperattenuation area in CTHA and hypoattenuation area in CTAP. It has been reported that the presence of Kupffer cells could be evaluated, and this was defined by a hyper-intensity area in the T2* image of SPIO-MRI as a typical imaging finding of HCC. Gd-EOB-DTPA MRI is a liver-specific contrast-enhanced agent, and hypointensity in the hepatobilliary phase is a typical imaging finding. We started to perform Gd-EOB-DTPA MRI instead of SPIO-MRI from March 2008, because it was reported that the sensitivity of Gd-EOB-DTPA MRI was superior to SPIO-MRI for the diagnosis of HCC.

Tumor Biopsy and RFA

There are 24 operators who participated in this study. They are specialized liver physicians who have great experiences in performing percutaneous ethanol injection for HCC, percutaneous tumor biopsy for liver tumor, percutaneous liver biopsy for hepatitis, percutaneous hepatobiliary drainage for obstructive jaundice, or percutaneous liver abscess drainage. A needle-guiding technique was used, consisting of an initial guided needle and a secondary outer needle (two-step insertion method). This method was reported by another center previously [18] and involves the initial insertion of a 21-gauge needle (Silux, Saitama, Japan) just adjacent to the tumor under real-time US guidance, and using this to insert a 14-gauge Daimon outer needle (Silux), also just adjacent to the tumor. After removal of the inner needle, an 18-gauge biopsy needle was inserted to obtain the tumor tissue sample. After removal of the biopsy needle, a 17-gauge cooled-tip electrode was inserted into the targeted tumor. The electrode, with a 2- or 3-cm exposed tip, was connected to a 480-kHz RF Generator (Radionics, Burlington, Mass., USA), which produces 200 W at 50 Ω of impedance [19, 20]. The equipment also allows the measurement of power output, tissue impedance and electrode tip temperature. A tip temperature of 10–20°C was maintained by infusion of chilled water through a peristaltic pump. After insertion of the electrode into the tumor, ablation was performed at 60 W for the 3-cm exposed tip and 40 W for the 2-cm exposed tip. The power was increased to 140 W at a rate of 10–20 W/min. When a rapid increase in impedance was observed during thermal ablation, the output was reduced. The duration of a single ablation was 12 min. After RF exposure, the pump was stopped and the temperature of the needle tip was measured. When the temperature of the electrode tip was >60°C, ablation was defined as being sufficient. When the target nodule was >2 cm in diameter, multiple needle insertions and ablations were performed in 1 nodule to achieve complete necrosis. A session was defined as a single intervention consisting of ≥1 ablations performed on ≥1 tumors at the same time. After completion of nodule ablation, the intrahepatic needle track was treated by thermocoagulation to avoid needle track seeding. Finally, a mixture of gelatin sponge particles (Gelfoam®; Upjohn, Kalamazoo, Mich., USA) was injected into the puncture route. All procedures were completed within 15–20 min. After each session of RFA, a dynamic CT scan (section thickness 5 mm) was performed to evaluate the efficacy of ablation. Complete ablation of HCC was defined as non-enhancement of the lesion, including the whole surrounding liver parenchyma. The ablative margin was shown as the boundary between the low density area as ablated area and the isodensity area as surrounding normal liver parenchyma. The residual portion of the tumor was treated by additional RFA within a few days of the post-treatment CT scan. Follow-up consisted of monthly serial measurements of tumor markers [α-fetoprotein (AFP) and des-γ-carboxy prothrombin (DCP)], US examination every 2 months and dynamic CT every 3 months. We checked various complications of RFA with conventional contrast-enhanced CT and blood examination at day 1 after RFA.

Tumor Recurrence

Recurrence of HCC was defined as an early enhancement area on dynamic CT, concomitant with late wash out. Two types of recurrence, local tumor progression and distant intrahepatic recurrence, were identified. Local tumor progression was defined as an enhancing area located adjacent to the ablated area [21], while distant intrahepatic recurrence referred to the appearance of a new tumor in the liver, distant from the ablated area. Early recurrence was defined as a recurrence within 12 months of the initial RFA.

Immunohistochemistry

Immunohistochemistry using antibodies against K19 (1:100, BA17, Dakocytomation, Glostrup, Denmark) was performed on paraffin-embedded sections from 246 needle biopsy specimens. The slides were reviewed by 2 independent pathologists (M. Komuta and M. Sakamoto). Expression of K19 was considered positive if >5% of tumor cells were stained according to the expected pattern of reactivity.

Statistical Analysis

Categorial variables were compared with the χ^2 test and continuous variables with the Mann-Whitney test; a p value <0.05 was considered statically significant. Continuous variables were expressed as the mean ± standard deviation. The imaging findings were compared with the χ^2 test between K19-positive and -negative patients. Overall survival was defined as the interval between treatment and death or the date of the last follow-up or the date of the most recent follow-up visit. Probability of recurrence-free survival was defined as the interval between treatment and the date of HCC recurrence.

Univariate analysis was performed to identify clinical and biological parameters (sex, age, etiology, prothorombin activity, albumin, bilirubin levels, Child-Pugh class, serum AFP level, serum DCP level) and tumor factors (size, number, tumor stage, tumor differentiation, K19 expression) predicting overall survival, recurrence-free survival and the interval beyond the Milan criteria.

Survival curves were computed according to the Kaplan-Meier method and compared by the log-rank test. All variables with a p value <0.05 were subjected to multivariate analysis by Cox's